INTERNATIONAL JOURNAL FOR NUMERICAL METHODS IN FLUIDS, VOL. 1, 237–272 (1981)

# COMPUTATION OF WAVE FIELDS IN THE OCEAN AROUND AN ISLAND

OVE SKOVGAARD

*Laboratory of Applied Mathematical Physics (LAMF), Bldg. 303, Technical University of Denmark, DK-2800 Lyngby, Denmark*

IVAR G. JONSSON

*Institute of Hydrodynamics and Hydraulic Engineering (ISVA), Bldg. 115, Technical University of Denmark, DK-2800 Lyngby, Denmark*

## SUMMARY

A linear wave equation correct to first order in bed slope is used to calculate the wave field in the sea around an idealized island. This is of circular cylindrical shape and is situated on a paraboloidal shoal in an ocean of constant depth (Figure 1). The sides of the island are assumed fully reflecting. The incident waves are plane and periodic. Wave periods up to 30 min are investigated, and the Coriolis force is neglected. The solution of the wave equation is represented by a finite Fourier series, and a large number of very accurate numerical computations are carried through. The results appear partly in figures showing amplitude and phase angle curves (in some cases extending to the water area of constant depth outside the shoal), partly in figures showing amplitude *vs* wave period in fixed points. Comparison with solutions to the linearized long-wave equation is made, and the validity range of the corresponding shallow water theory is given. The influence of the shoal is studied by investigating the wave field around an island in an ocean of constant depth. New criteria are given for the applicability of a geometrical optics approach (i.e. refraction). Complete numerical refraction solutions for points at the shoreline (corresponding to many wave orthogonals ending at the point) for shallow water waves, as for the general case, demonstrate the inadequacy of this approach for long-period waves (seismic seawaves: tsunamis). All non-linear effects, including dissipation, are excluded.

KEY WORDS Diffraction Refraction Gravity Water Waves Wave Equation Homma's Island Tsunamis

## 1. INTRODUCTION

A seismic sea wave, a so-called tsunami (Japanese for 'harbour wave'), consists of a series of waves that approaches the coast with periods usually ranging from 5 to 90 min (Reference 1, p. 2). The lengths of these waves are of the order of hundreds of kilometres in the deep ocean, while here their amplitudes are usually of the order of a metre. They are therefore difficult to detect from the air or from ships. Near land, however, the tsunamis will build up in height due to the decrease in water depth. At the same time the amplitude can be further amplified because of lateral convergence and reflections. The wavelength will be reduced in shallower water.

The final run-up of tsunamis is a highly non-linear phenomenon. In this study, however, we shall investigate the modification of the tsunami wave over that area near the coast, where linear theory can be used, i.e. excluding the final run-up.

A tsunami can also be generated by non-seismic causes, such as landslides and nuclear explosions. Therefore Murty (Reference 1, p. 1) cites the more general definition by van

0271–2091/81/030237–36$03.60

*Received 12 August 1980*
*Revised 3 March 1981*

Dorn: 'Tsunami is the Japanese name for the gravity wave system formed in the sea following any large-scale, short duration disturbance of the free surface'. Most of the current knowledge about tsunamis and tsunami engineering is excellently reviewed by Murty,[1] and by Camfield.[2]

We will calculate the transformation of a small, regular, and plane incident wave caused by an idealized island of circular cylindrical form, situated on a paraboloidal shoal in an infinite ocean of constant depth, see Figure 1. (To investigate the influence of the shoal, we have also looked briefly at an island without a shoal, see Section 5.)

The water depths, $h$, are

$$\begin{aligned} h &= \alpha r^2 \quad \text{for} \quad r_a \le r \le r_b \quad \text{and} \quad 0° \le \theta < 360° \\ h &= h_b (= \alpha r_b^2) \quad \text{for} \quad r_b \le r < \infty \quad \text{and} \quad 0° \le \theta < 360° \end{aligned} \tag{1}$$

The shoreline radius is $r_a = 10$ km, the outer radius of the shoal is $r_b = 30$ km, and the depth $h_b = 4{,}000$ m. Thus shoreline depth is $h_a = h_b (r_a/r_b)^2 = 4{,}000/9 \approx 444$ m. (Generally subscript $a$ denotes a value at the shoreline, and subscript $b$ denotes a value at the outer boundary of the shoal.) The factor of proportionality, $\alpha$, in (1) becomes $\alpha = 4/9 \times 10^{-5}$ m$^{-1}$.

This type of island is seemingly accepted as being representative of a 'Pacific island'.[3,4] Tsunami amplification over other depth profiles has been discussed by Meyer,[5] Smith and Sprinks,[6] and Kriegsmann,[7] and experiments have been performed by Williams and Kartha[8] and Provis.[9]

The present paper is a sequel to papers by Jonsson *et al.*[10] (hereafter referred to as *paper I*), where we restricted the presentation to the wave field at the shoreline, including some shallow water refraction calculations, and by Jonsson and Skovgaard[11] (hereafter referred to as *paper II*), where we looked at the wave field over the shoal for wave periods up to 240 s, including a few intermediate depth refraction calculations for the shoreline.

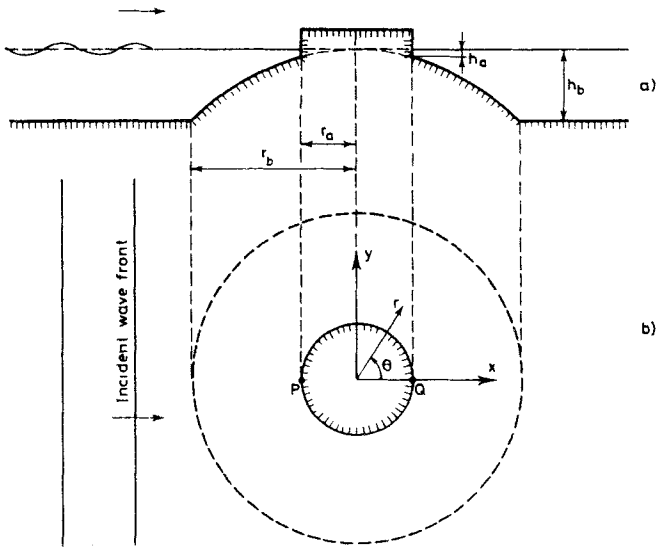


Figure 1. Sketch of the idealized island on a paraboloidal shoal: (a) vertical; (b) horizontal

The purpose of the paper is therefore threefold. Firstly to investigate the wave field (amplitudes and phase angles) *outside* the shoal, i.e. to study the 'disturbance' out in the deep ocean due to the presence of the island. Among other things it will be seen here that amphidromic points (i.e. points where the amplitude is always vanishing) can also be found on constant water depth, even in the absence of a Coriolis force. Secondly, we will look at the wave field over the shoal itself for one representative wave period $T$ larger than 240 s, viz $T = 480$ s. (In selected points at the shoreline the amplitude will be given as a continuous function of $T$.) For both cases above the (diffraction) wave field comes out as a solution to a linear so-called mild-slope wave equation, presented in Section 2. Thirdly, we shall look into the results of a 'vector addition refraction theory' for intermediate depth. Here the physical limitations of a refraction approach (i.e. geometrical optics) for long waves will be illustrated.

A discussion is given in paper I of other approaches to calculate 'waves around islands'.

Two points are selected for a more detailed investigation. One is the middle of the front face of the island; it is called point P. The other is the middle of the 'shadow' part of the island, point Q. Both points are shown in Figure 1.

In Appendix I we have made an investigation of the convergence rates of the series used in the diffraction solution. The computer and the programming language are referred to in Appendix II. In Appendix III the abbreviations used throughout the paper are summarized.

A number of figures from papers I and II are referenced in the text. Some of the key figures from these papers are therefore reprinted in Appendix IV.

## 2. ASSUMPTIONS AND DEFINITIONS

The incident surface gravity waves are assumed to be plane, time-harmonic, and of small amplitude. The Coriolis force is neglected, which is justified for the considered higher end of the tsunami frequency range. The sides of the island are assumed fully reflecting. All non-linear effects (including dissipation) are neglected.

The diffraction of a simple time-harmonic surface gravity wave over a gently sloping sea bed is governed by the following reduced mild-slope wave equation.[12-16]

$$\nabla \cdot (cc_g \nabla \eta) + cc_g k^2 \eta = 0 \tag{2}$$

where $\nabla$ is the horizontal gradient operator $(\partial/\partial x, \partial/\partial y)$ or $(\partial/\partial r, r^{-1}\partial/\partial\theta)$, $c$ is the phase speed, $c_g$ is the group speed, $k = 2\pi/L$ is the wave number ($L = cT$ is wavelength), and $\eta = \eta(r, \theta)$ is the (complex) surface wave *amplitude*. $r$ and $\theta$ are defined in Figure 1.

Note that the instantaneous *complex* surface elevation is $\eta \exp(-i\omega t)$, where i is the imaginary unit, $\omega = 2\pi/T$ is the (constant) angular frequency, and $t$ is time. The instantaneous *real* surface *elevation* $\zeta$ is thus

$$\zeta = \mathrm{Re}\{\eta \exp(-i\omega t)\} \tag{3}$$

We define the *real* surface *amplitude* $A = A(r, \theta)$, and phase angle $\varphi = \varphi(r, \theta)$ (also real) by

$$\eta = A \exp(i\varphi) \tag{4}$$

i.e. we have from (3).

$$\zeta = A \cos(\varphi - \omega t) \tag{5}$$

Phase angle is still determined less an arbitrary constant. This is remedied by demanding that $\varphi$ be zero in the far field at $\theta = \pm 90°$ for $t = 0$. In other words, $\varphi$ is the phase angle at that instant, when the undisturbed wave crest passes through the centre of the island.

The real amplitude of the incoming wave is called $A_i$. In the amplitude graphs we have depicted the *relative* amplitudes $A/A_i$.

The phase speed $c$ is determined by the classic implicit dispersion relation for small amplitude water waves

$$c = \sqrt{\left(\frac{g}{k}\tanh kh\right)} \tag{6}$$

in which g is the gravity acceleration, and $h = h(r, \theta)$, the water depth. The group speed $c_g$ is determined by

$$c_g = \frac{1}{2}c\left(1+\frac{2kh}{\sinh 2kh}\right) \tag{7}$$

For very long waves (in practice $h/L < 0{\cdot}05$), (2) reduces to the linearized long-wave equation

$$\nabla\cdot(h\nabla\eta)+hk^2\eta = 0 \tag{8}$$

In this case there is no dispersion and the phase and group speeds are given by

$$c = c_g = \sqrt{(gh)} \tag{9}$$

For calculations involving (6) and (7), we use the acronym IDT, which stands for Intermediate Depth Theory. For calculations involving (9) we use the acronym SWT, which stands for Shallow Water Theory.

For constant water depth, or in deep water (in practice $h/L > 0{\cdot}5$), (2) reduces to the Helmholtz equation

$$\nabla^2\eta + k^2\eta = 0 \tag{10}$$

Equation (2) is correct to first order in both wave amplitude and bed slope.[16]

The applicability of a time-stepping approximate finite difference method, which is more related to practice, is tested in a concurrent publication.[17]

The deep water wavelength $L_0$ emerges from (6) with $\tanh kh = 1$,

$$L_0 = \frac{g}{2\pi}T^2 \tag{11}$$

## 3. THE GLOBAL WAVE FIELD

One of the new features of this paper is the calculation and presentation of the wave field also outside the shoal, i.e. in the area of constant water depth far away from the island. This is important for several reasons. One is that in connection with the possible application of a general mathematical/numerical model on tsunami response[17] we must know the rate of decay of the oscillations of the water surface around the island. In this paper this extended investigation will be presented in graphs and tables.

Another important application of such very accurate solutions is that they can serve as a check for more general numerical schemes. In order to facilitate such a check two numerical test solutions are tabulated in Table I. In the table relative amplitude $A/A_i$ and phase angle $\varphi$ are given for two periods ($T = 120$ s and 480 s), for seven values of azimuth $\theta$ ($= 0°$, 30°, 60°, 90°, 120°, 150° and 180°), and for three values of relative distance, $r/r_a$ ($= 1$, 3 and 9). The values in Table I(a) are calculated using shallow water theory, and the values in Table

Table I. Diffraction solution for the wave field over the shoal, and on constant water depth. The values of phase angle $\varphi$ are chosen in the interval $0° \leq \varphi < 360°$. Integers in parentheses indicate powers of 10 by which the following numbers are to be multiplied

(a) Using SWT, (8), T = 480 sec.

| | $\theta = 0°$ | $\theta = 30°$ | $\theta = 60°$ | $\theta = 90°$ | $\theta = 120°$ | $\theta = 150°$ | $\theta = 180°$ |
|---|---|---|---|---|---|---|---|
| $(A/A_i)_{r=r_a}$ | 2.3692 | 1.7783 | 1.5253 | 2.6996 | 3.4019 | 3.5147 | 3.4886 |
| $(\varphi^o)_{r=r_a}$ | (+2)1.4971 | (+2)1.3245 | (+1)5.9653 | (+1)1.5667 | (+2)3.5518 | (+2)3.4112 | (+2)3.3548 |
| $(A/A_i)_{r=3r_a}$ | 1.5321 | 1.0055 | (-1)8.0589 | 1.3347 | (-1)9.9241 | (-1)5.1496 | (-1)4.9201 |
| $(\varphi^o)_{r=3r_a}$ | (+2)1.9384 | (+2)1.7399 | (+1)7.0596 | (+1)2.0287 | (+2)3.4407 | (+2)2.8704 | (+2)2.4844 |
| $(A/A_i)_{r=9r_a}$ | 1.2252 | (-1)5.7584 | 1.0596 | (-1)9.6740 | 1.1041 | (-1)7.7372 | 1.0993 |
| $(\varphi^o)_{r=9r_a}$ | (+1)2.6548 | (+2)3.3426 | (+2)1.6076 | (+2)3.4795 | (+2)2.0800 | (+1)4.6236 | (-1)2.2356 |

(b) Using IDT, (2), T = 120 sec.

| | $\theta = 0°$ | $\theta = 30°$ | $\theta = 60°$ | $\theta = 90°$ | $\theta = 120°$ | $\theta = 150°$ | $\theta = 180°$ |
|---|---|---|---|---|---|---|---|
| $(A/A_i)_{r=r_a}$ | 3.6932 | 2.6044 | 1.1589 | 2.0652 | 2.4398 | 3.1314 | 2.1950 |
| $(\varphi^o)_{r=r_a}$ | (+2)1.4091 | (+2)3.1459 | (+1)7.3373 | (+2)2.2080 | (+1)9.2018 | (+2)3.5820 | (+2)3.5608 |
| $(A/A_i)_{r=3r_a}$ | (-1)8.9702 | (-1)6.9695 | (-1)1.0274 | 1.6081 | (-1)8.4291 | 1.1834 | 1.2761 |
| $(\varphi^o)_{r=3r_a}$ | (+2)1.1853 | (+2)2.6433 | (+1)5.4907 | (+2)3.3509 | (+2)1.0777 | (+2)2.0168 | (+2)1.8384 |
| $(A/A_i)_{r=9r_a}$ | (-1)6.8321 | (-1)9.3916 | 1.3645 | 1.0760 | 1.2232 | (-1)9.4119 | 1.4079 |
| $(\varphi^o)_{r=9r_a}$ | (+1)1.8679 | (+2)3.2553 | (+2)1.0865 | (+2)3.5520 | (+2)2.5145 | (+2)3.4289 | (+2)1.4783 |

I(b) using intermediate depth theory. The table is an extension of paper I, Table 2, which stopped at the base of the shoal ($r/r_a = 3$). Also another SWT period is chosen here, $T = 480$ s instead of $T = 410{\cdot}47\ldots$ s.

### 3.1. *The shallow water theory (SWT)*

In order to calculate the wave field over the area in question, we solve the partial differential equation (8), the shallow water wave equation. The boundary conditions are full reflection at the island ($r = r_a$), and Sommerfeld's radiation condition at infinity (for the scattered part of the wave field). See paper I for details.

Because of the rotational symmetry of the bathymetry, we can apply the method of separation of variables.

*Over the shoal* ($r_a \leq r \leq r_b$) the solution for the complex amplitude is

$$\eta = \sum_{n=0}^{\infty} R_n(r) \cos(n\theta) \qquad 0 \leq \theta < 360^\circ \tag{12}$$

where the functions $R_n(r)$ ($n = 0, 1, 2, \ldots$) are solutions to linear two-point boundary value problems. These ordinary differential equations were solved by Homma,[3] see paper I, pp. 473–476 for details. Angle $\theta$ is defined in Figure 1.

*Outside the shoal* ($r \geq r_b$) the wave field is the sum of an incident and a scattered wave field, i.e.

$$\eta = \eta_i + \eta_{sc} \tag{13}$$

with

$$\eta_i = A_i \sum_{n=0}^{\infty} \varepsilon_n i^n J_n(k_b r) \cos(n\theta) \tag{14}$$

$$\eta_{sc} = \sum_{n=0}^{\infty} C_n H_n^{(1)}(k_b r) \cos(n\theta) \tag{15}$$

In these equations $A_i$ is the amplitude (real) of the incoming wave, $\varepsilon_n$ is the Neumann factor (i.e. $\varepsilon_n = 1$ for $n = 0$, and $\varepsilon_n = 2$ for $n \neq 0$) i is the imaginary unit, $J_n$ are Bessel functions of $n$th order and first kind, $k_b = 2\pi/L_b$, the wave number for $r \geq r_b$, $C_n$ are integration constants, and $H_n^{(1)}$ are Hankel functions of the $n$th order and first kind.

At $r = r_b$ there is continuity in $\eta$ and in its first derivative with respect to $r$. Using the former condition we find from (12) and (13) for the determination of $C_n$

$$C_n = \frac{1}{H_n(\tau)} [(R_n)_{r=r_b} - A_i \varepsilon_n i^n J_n(\tau)] \qquad n = 0, 1, 2, \ldots \tag{16}$$

where we have dropped the superscript (1) on $H$, and further $\tau \equiv k_b r_b$. Functions $(R_n)_{r=r_b}$ are determined by Homma's[3] solution (SWT, see (3.19) in paper I). Inserting the results in (16) yields

$$C_n = \frac{A_i \varepsilon_n i^n}{H_n} \left[ \frac{i\left[\rho^{\alpha_n} + \dfrac{\alpha_n - 1}{\alpha_n + 1} \rho^{-\alpha_n}\right] \dfrac{2}{\pi} \rho^{\alpha_n}}{\rho^{2\alpha_n}[(1-\alpha_n)H_n + \tau H_n'] + \dfrac{\alpha_n - 1}{\alpha_n + 1}[\tau H_n' + (1+\alpha_n)H_n]} - J_n \right] \qquad n = 0, 1, 2, \ldots \tag{17}$$

where $\rho \equiv r_b/r_a$, $\alpha_n \equiv \sqrt{(1 + n^2 - \tau^2)}$, and we have dropped the argument $\tau$ of the Bessel function and of the Hankel function and its derivative (i.e. here $H_n' = (dH_n^{(1)}(k_b r)/d(k_b r))_{r=r_b}$).

The complete solution outside the shoal hereafter emerges from (13)–(15) with (17) inserted in the latter equation.

Some results are depicted in Figures 2 and 3. By comparing the two it is seen that amplitudes in the 'shadow' of the island are much smaller for the small period than for the large one, as expected. Conversely, reflection along the centreline in front of the island is highest for the small period, and the decay rate quite small. Maxima and minima are indicated along the boundaries of the depicted area. It appears that even some wavelengths away from the island the incident wave is quite perturbed. This is also illustrated by Figure 4, in which positions of maxima and minima are indicated.

It is seen in Figure 2 that amphidromic points can also exist in the constant depth region. This was also found by Provis,[9] who considered a conical island in an ocean of constant depth.

A more detailed picture of the phase structure over the shoal for $T = 240$ s is found in Figure 7, where $\Delta\varphi$ is only 30°. Details of the wave field over the shoal and in its immediate vicinity for $T = 480$ s are presented in Figure 5, which is an enlarged version of the central part of Figure 3.

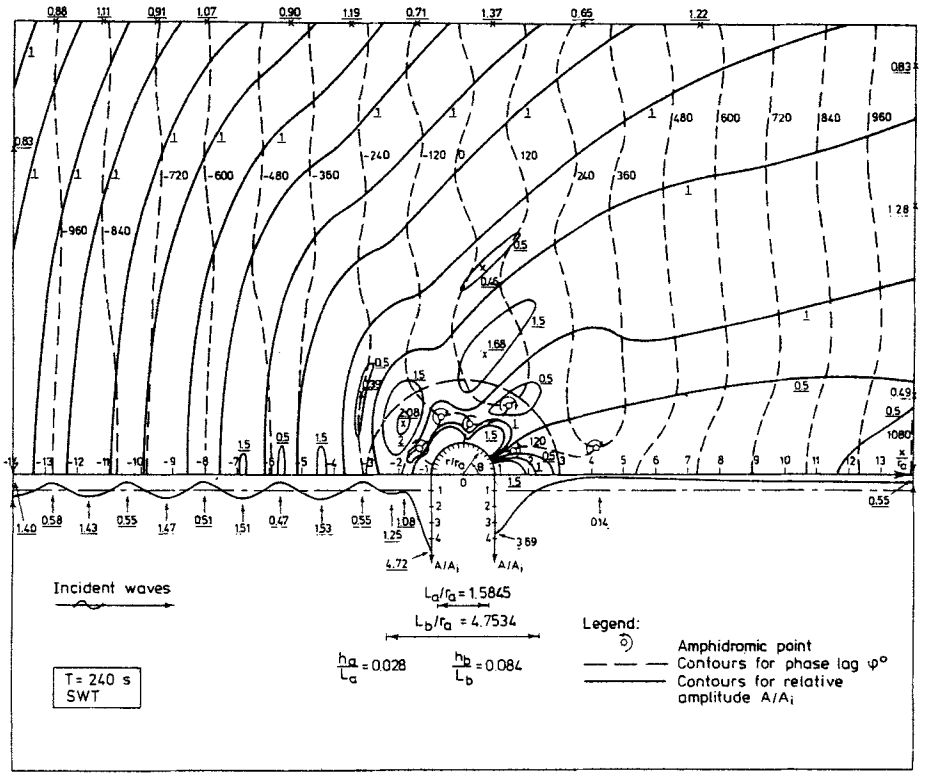


Figure 2. Contours for relative amplitude $A/A_i$ and phase angle $\varphi$ over the shoal and on constant water depth outside. $T = 240$ s. The interval between $A/A_i$-curves is 0·5 (curves over $A/A_i = 1{\cdot}5$ not shown), and between $\varphi$-curves is 120°. Underlined numbers are $A/A_i$

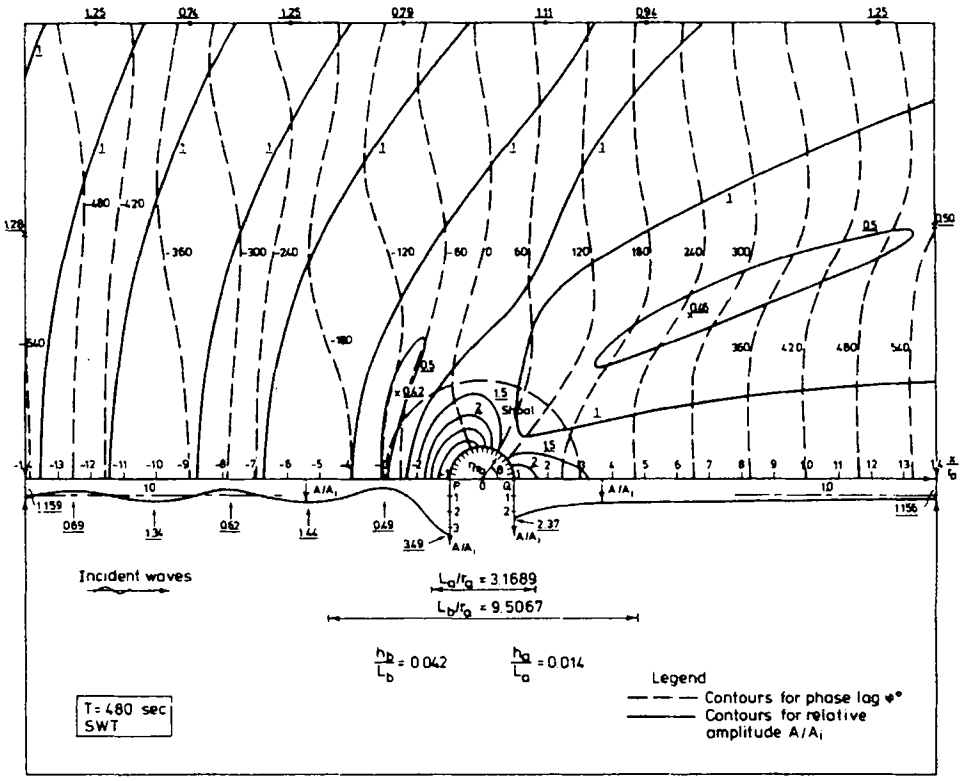


Figure 3. Contours for relative amplitude $A/A_i$ and phase angle $\varphi$ over the shoal and on constant water depth outside. $T = 480$ s. The interval between $A/A_i$-curves is 0·5, and between $\varphi$-curves is 60°. Underlined numbers are $A/A_i$

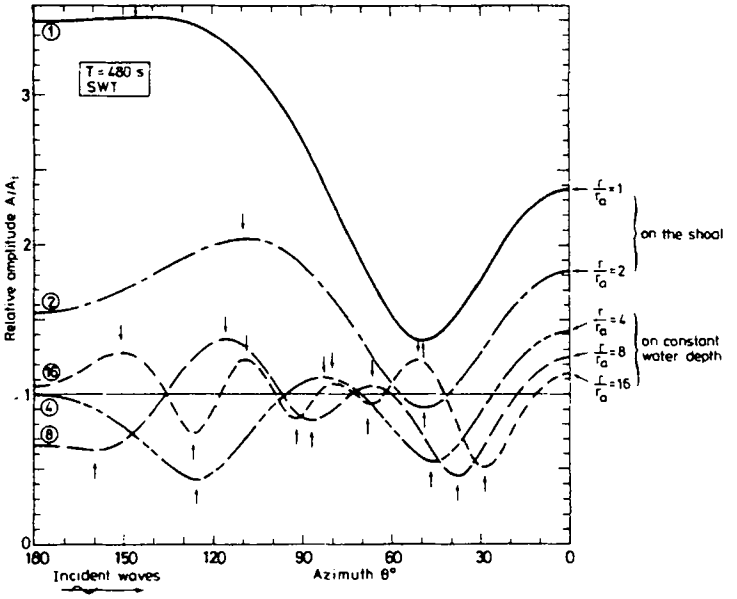


Figure 4. Relative amplitude $A/A_i$ *vs* azimuth $\theta$° along half circles. $T = 480$ s

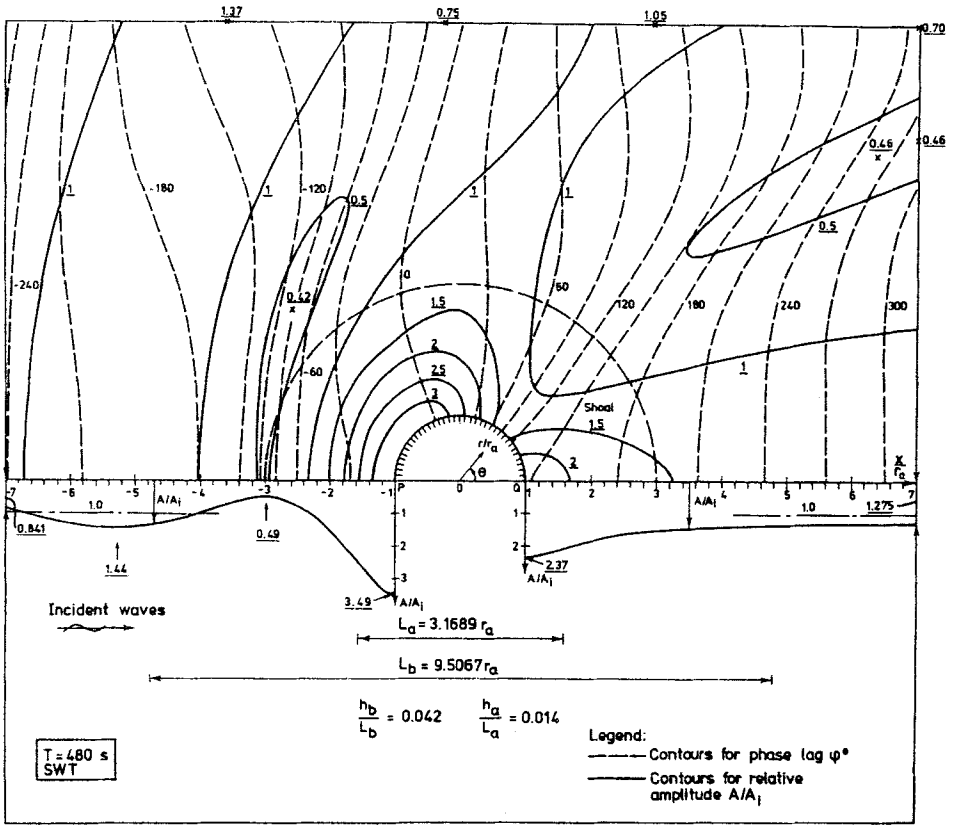


Figure 5. Contours for relative amplitude $A/A_i$ and phase angle $\varphi$ over the shoal and on constant water depth outside. $T = 480$ s. The interval between $A/A_i$-curves is 0·5, and between $\varphi$-curves is 30°. Underlined numbers are $A/A_i$

### 3.2. *The intermediate depth theory (IDT)*

The wave field is here a solution to the general wave equation (2). Over the shoal it is here calculated for two periods, $T = 120$ s and 240 s, see Figures 6 and 7.

In Figure 6 we have shown the wave field for $T = 120$ s. Only the constant phase lines are depicted; the corresponding amplitude curves are given in paper II, Figure 3, and in Appendix IV. The solution is given by an expansion analogous to (12), see paper I, pp. 473–475 and 481–483, and paper II, pp. 44–46, for details. There are many amphidromic points over the shoal for this short period, 46 ($= 2 \times 23$) in all.

It appears from paper I, Figure 6, and paper II, Figure 4 (also Appendix IV), and paper II, Figure 5 (also Appendix IV), as from Figure 9 in the present paper (the point Q in Figure 1), that it is meaningless to use SWT for a period of 120 s. There is therefore no comparison attempted with a shallow water solution in Figure 6.

This is done for the double period, however, $T = 240$ s in Figure 7. (The SWT part is a 'blow-up' of Figure 2). Also here only the constant phase lines are given; the corresponding comparison of amplitudes is shown in paper II, Figure 6, and in Appendix IV. As could be

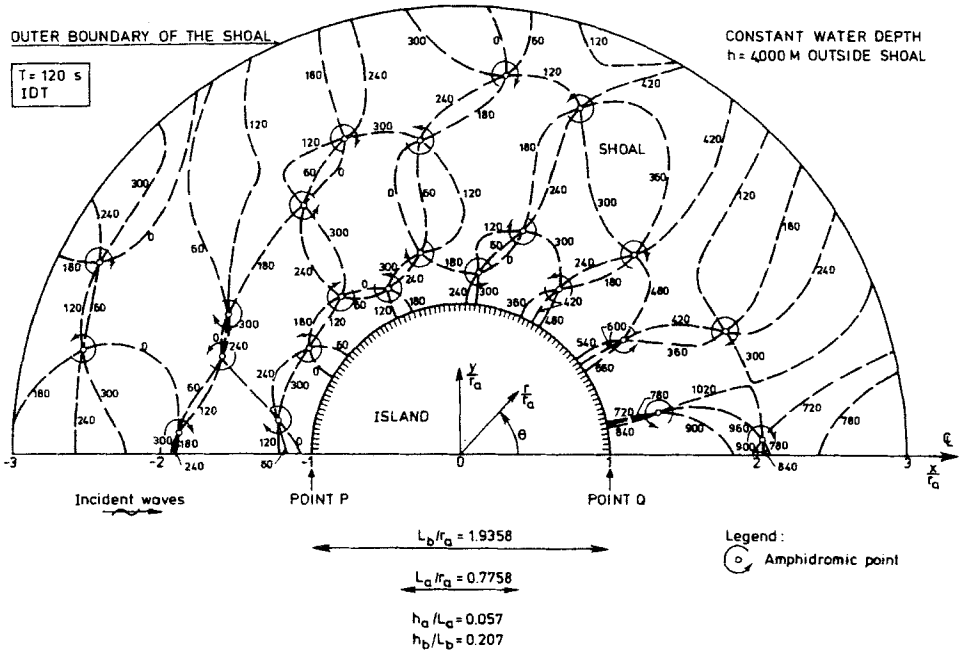


Figure 6. Contours for phase angle $\varphi$ over the shoal. $T = 120$ s. The interval between the $\varphi$-curves is 60°

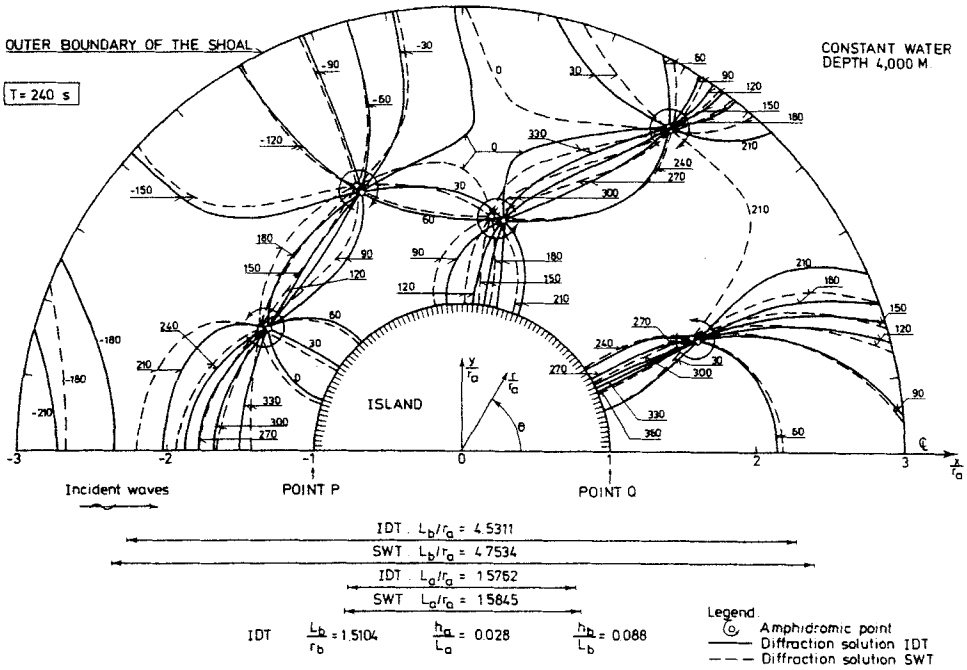


Figure 7. Contours for phase angle $\varphi$ over the shoal corresponding to both IDT and SWT. $T = 240$ s. The interval between the $\varphi$-curves is 30°

anticipated from Figure 9, the difference between the two solutions is not large. This can also be seen from the closeness of the two sets of amphidromic points. The number of these over the shoal has fallen from the 46 for $T = 120$ s to now only 10 ($= 2 \times 5$). (The number of amphidromic points is naturally closely connected with the 'frequency' of the oscillation of a curve like that in Figure 9: By analogy with the response curve for an 'organ pipe', it appears that the number of amphidromic points must increase with increasing frequency.)

## 4. THE LOCAL WAVE FIELD

In this section we shall concentrate on conditions at the shoreline ($r = r_a = 10{,}000$ m), with special emphasis on the points P and Q (see Figure 1). The point P is situated at the middle of the 'illuminated' part of the island, while the point Q is at the middle of the 'shadow' part. In particular the short wave limit at these two points will be illustrated and discussed.

### *4.1. The diffraction solution*

The IDT-solution at the island (i.e. the solution to (2) for $r = r_a$) is given in Figure 8 for $T = 120$ s. This relatively short period results in many amplitude peaks at the shoreline. The number of peaks decreases with increasing period $T$, see Figure 2 in paper I and Appendix IV, and Figure 7 in paper II. Note that for this period the amplitude in the shadow point Q exceeds that in the illuminated point P. The refraction solutions in the figure are dealt with in Section 4.2.

The relative amplitude at the point P as a function of period was depicted in detail as Figure 6 in paper I, and as Figure 4 in paper II (also Appendix IV). A similar figure for the point Q is presented here as Figure 9, which is a 'blow-up' of the first 500 s of the 1,800 s range in Figure 5 in paper II (also in Appendix IV). A comparison with the just mentioned figures for the point P shows that the mean amplitudes (averaged over one oscillation) are about the same for the points Q and P in the period range 100–400 s. However, oscillations

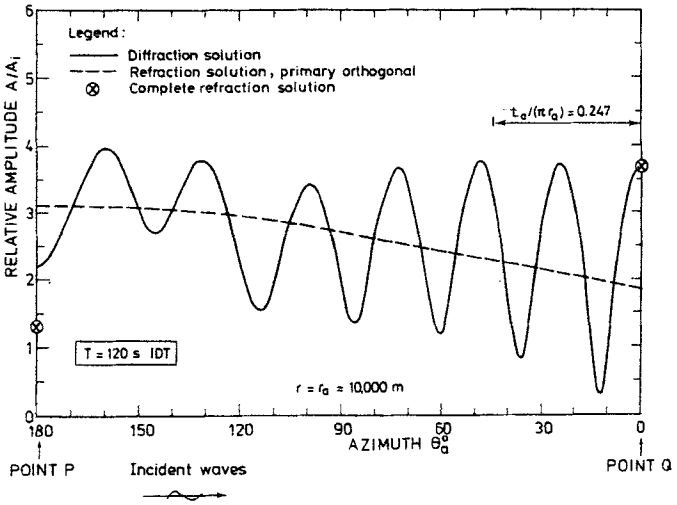


Figure 8. Relative amplitude $A/A_i$ at shoreline *vs* azimuth $\theta_a^\circ$

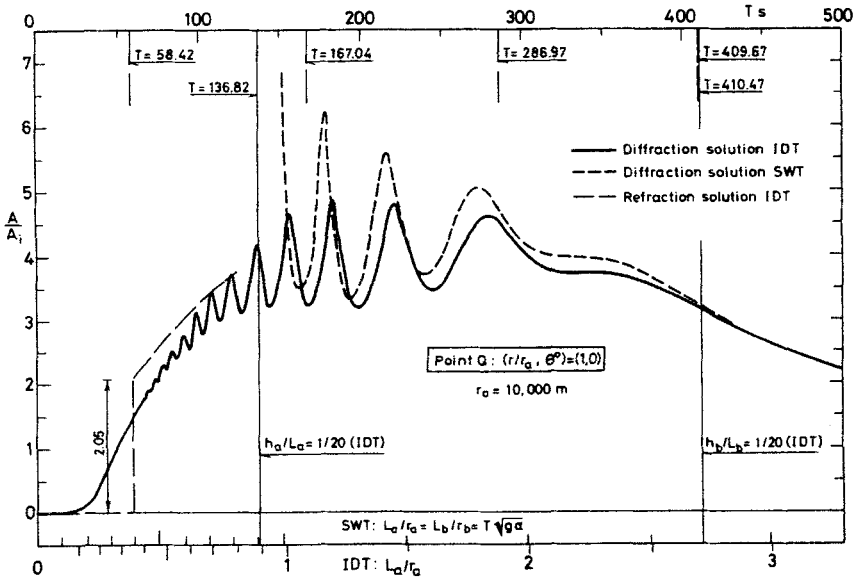


Figure 9. Relative amplitude $A/A_i$ at the point Q $[(r/r_a, \theta_a^\circ) = (1, 0)]$ *vs* wave period $T$ and relative wavelength $L_a/r_a$

are much smaller at the point Q, oscillation heights being only about half the size of those at the point P.

The accuracy of the shallow water approximation can also be read from Figure 9. The usually accepted shallow water limit $h/L = 1/20$ yields for $h = h_b = 4{,}000$ m a limiting period of about 410 s. The SWT-solution (i.e. the solution to (8)) is seen to be very accurate here. It can be concluded, therefore, as in paper II, that the shallow water wave equation (8) gives a good prediction of amplitudes near the shoreline for tsunami periods larger than about 7 min, as long as linear theory holds. If a high accuracy is not needed, one can even choose a lower limit, say 5 min.

For smaller periods the SWT approximation becomes rapidly more inaccurate. It appears from Figure 9 that although the discrepancy is not totally one-sided, the general trend is the SWT solution exaggerating the amplitudes. This is very noticeable for the peak values at the 'resonance' periods.

The situation in the short wave limit for the point Q is illustrated in Figure 10.

As expected, wind waves and swell ($T < 20$ s) do not effectively reach the point Q. As the deep water limit at the shoreline $h_a/L_a = 0{\cdot}50$ is passed, however, the amplitude grows rapidly. This is because the waves are 'bent' around the island as soon as they 'feel bottom', since the phase speed is smallest at the island, where the water depth is smallest. Thus the increase in amplitude is expected to be smaller had the water depth been constant. This appears from the figure, which further demonstrates that the two cases give almost identical results for 'deep water periods'.

A similar presentation is given in Figure 11 for the point P. As expected, the situation for deep water periods corresponds very nearly to just full reflection ($A/A_i \approx 2$). Two effects influence the amplitude as we pass the deep water limit towards larger periods. The

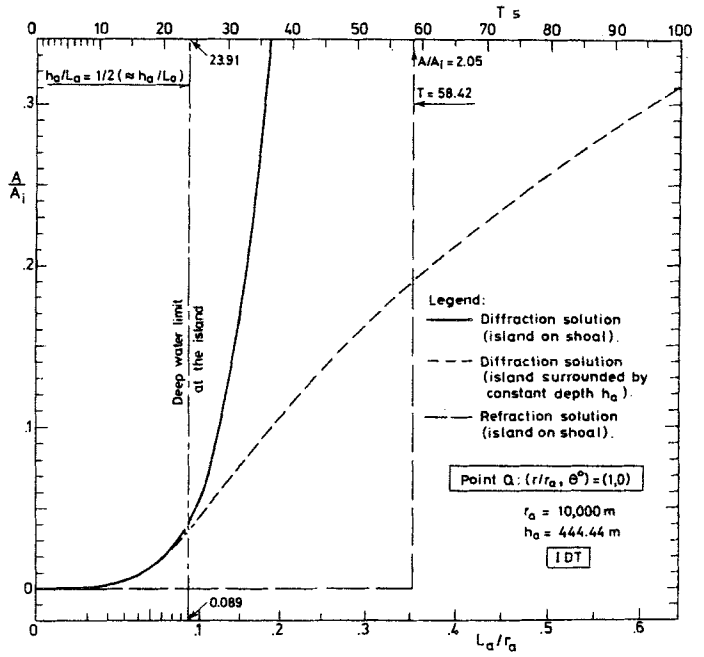


Figure 10. Relative amplitude $A/A_i$ at the point Q for small periods $T$

'convergence' of the waves tends to increase the height; the 'shoaling' tends to decrease the height in the beginning, since group speed (7) has a maximum for $2\pi h/L_0 = 1$. (The former effect is the strongest for the point Q.) Therefore a drop in the amplitude curves is experienced as we pass the deep water limit. Hereafter the two effects go in the same direction, the amplitude grows fast and starts to oscillate visibly for $T \approx 35$ s. The solution for constant depth $h = h_a$ naturally does not exhibit such behaviour, since the two effects mentioned are not present here. (The terms 'convergence' and 'shoaling' both in fact belong to geometrical optics, see (23). The concepts are useful, however, for a qualitative description, and as can be seen from the figure, also quantitatively for small periods ($T \lesssim 35$ s), where the diffraction and refraction solutions almost coincide.)

### *4.2. The refraction solution*

In paper I it was shown that in the shallow water case (SWT) the orthogonals are always logarithmic spirals over the shoal, so that all incoming waves meeting the shoal are 'trapped'. This means that the incoming orthogonals in the range $-r_a < y < r_a$ (see Figure 1) will all eventually end at the shoreline, the outermost having first whirled many times around the island. It was further shown that the complete SWT shoreline amplitude everywhere is the (complex) sum of an infinite number of individual complex amplitudes, each one corresponding to its logarithmic spiral. The results were shown to be in poor agreement with the diffraction solution (paper I, Figure 7, also in Appendix IV), and the sum diverged for $2\pi r_a/L_a$ being an integer. IDT-formulae were presented, but no numerical results were given, except for the primary orthogonal reaching the point P.

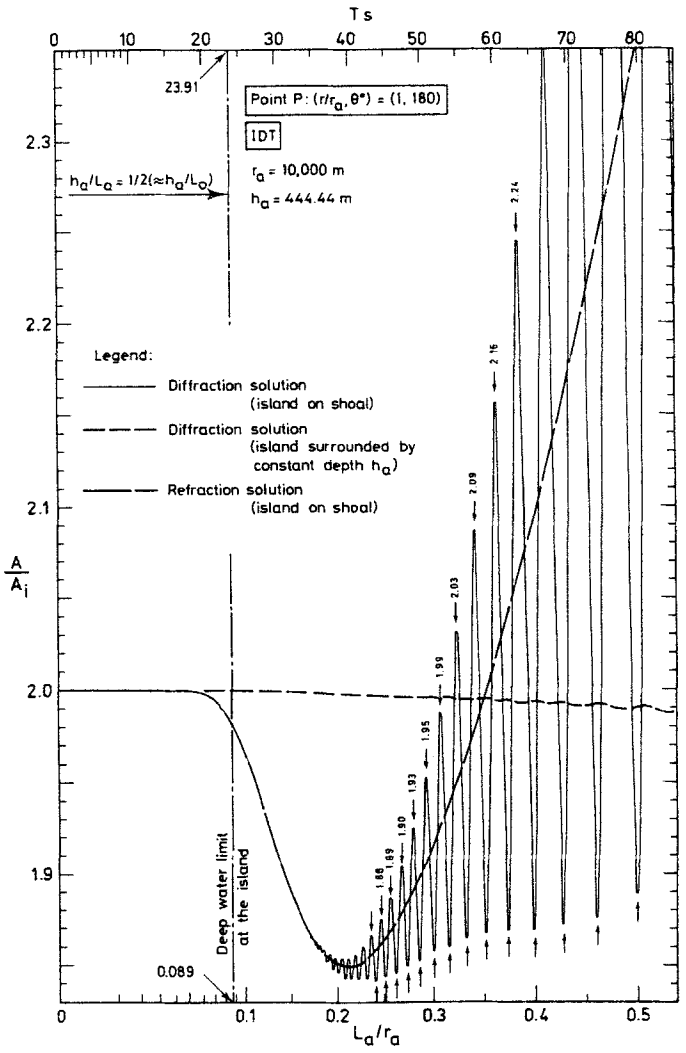


Figure 11. Relative amplitude $A/A_i$ at the point P for small periods $T$

In paper II it was shown that the IDT refraction solution results in a *finite* number of contributions to the amplitude everywhere, the number increasing with period, and the spirals are no longer logarithmic. For the point P the first four limiting periods were presented, i.e. the periods where the number of orthogonals is suddenly increased by two. Some of the corresponding limiting orthogonals were shown in Figure 9, and a few numerical values given in Figure 4 (paper II); the latter figure is also presented in Appendix IV. The corresponding vector addition diagrams were not shown, however. Problems concerning points in the 'geometrical shadow' were deferred for later treatment, and so this will also be dealt with here.

In this section we shall deal briefly with the fundamentals of the refraction approximation (when are geometrical optics methods reliable?). We shall furthermore go deeper into vector addition problems.

Let us first illustrate the effect of the period by considering Figures 12, 13 and 14.

For the very short waves (Figure 12), only the orthogonals passing close to the island will experience an appreciable change of direction; the shoal acts as a weak 'condenser lens', and there is no real 'trapping'. As a result the shadow part of the island is virtually unaffected by the waves. (Figure 10 shows that the relative amplitude at the point Q is really about 0·12 for $T = 30$ s.)

The 'medium' period chosen in Figure 13 corresponds to $h_a/L_a = 1/20$, i.e. shallow water waves at the island (but not further out). The figure shows an appreciable number of orthogonals being trapped by the shoal. However, in contrast to the shallow water case, the spirals are not logarithmic, and not all are trapped. For some $y$-value of the incoming wave in the region $26{,}100\text{ m} < y < 27{,}000\text{ m}$, the orthogonals start leaving the shoal without having touched the island. In Figure 14 the period is further increased, corresponding to $h_b/L_b = 1/20$, i.e. 'shallow water' everywhere. The orthogonal paths are therefore close to being logarithmic spirals (dashed curves) as shown. Three orthogonals hitting the point P are shown (corresponding, in reality, to a total of five because of symmetry). As can be seen from Figure 4 in paper II, the *total* number of orthogonals for the point P is seven for the period considered.

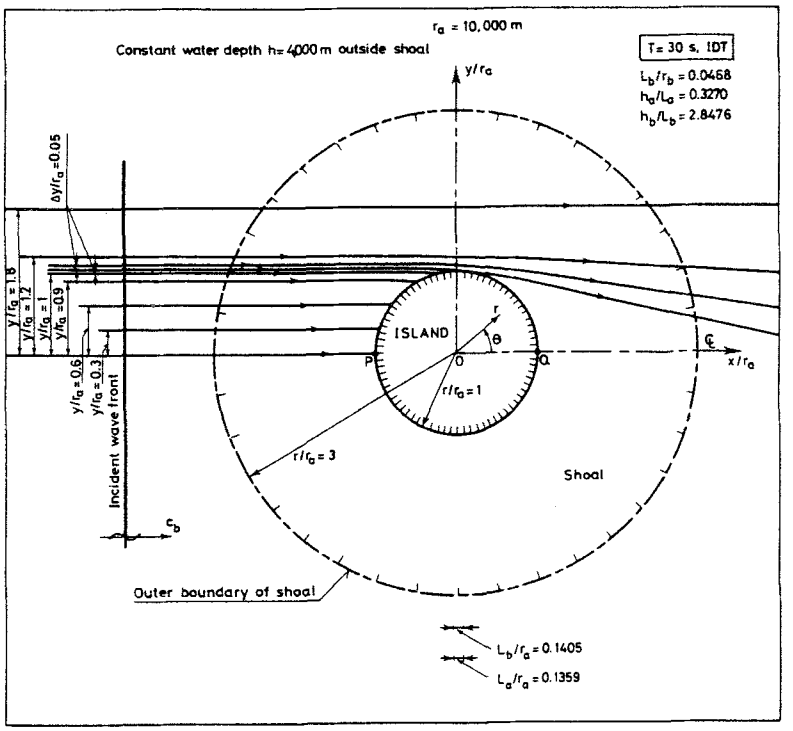


Figure 12. Orthogonal paths for $T = 30$ s

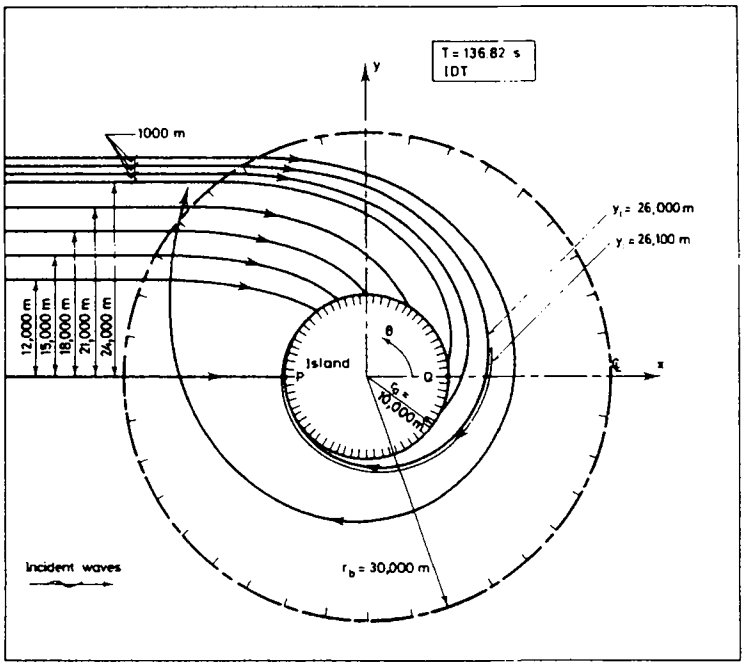


Figure 13. Orthogonal paths for $T = 136{\cdot}82$ s ($h_a/L_a = 1/20$). (The thin curve beginning to the right part of the figure corresponds to an incoming y-value of 26,100 m)

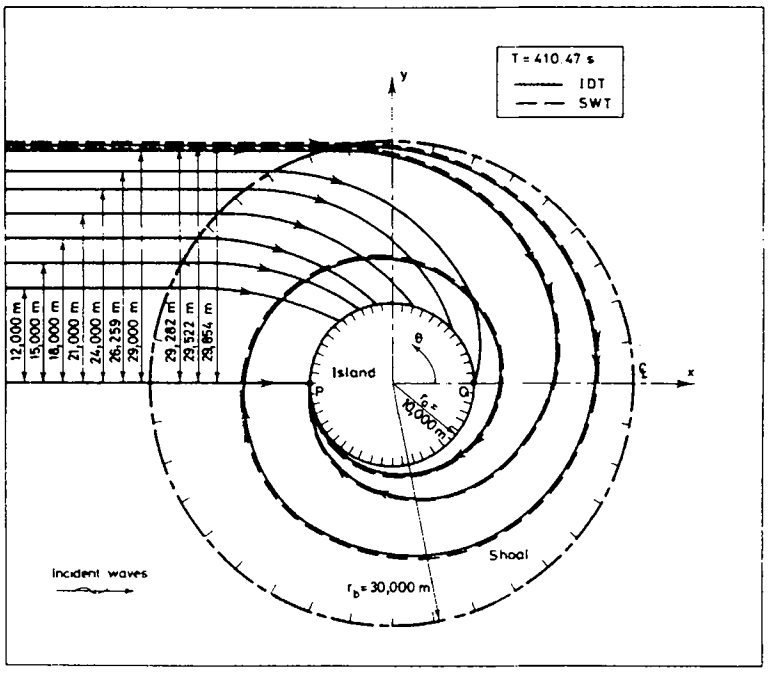


Figure 14. Orthogonal paths for $T = 410{\cdot}47$ s ($h_b/L_b = 1/20$)

A criterion for the applicability of a refraction approach can be found in the following way.[18] We seek a 'propagation solution' of the form

$$\eta = Ae^{-ikR} \tag{18}$$

to the wave equation (2) and investigate under which circumstances (18) can in fact be a solution. In (18) ('Debye's Ansatz', see Reference 19, pp. 10–11) $\eta = \eta(x, y)$ is the complex amplitude, and $A = A(x, y)$ is the physical amplitude (half wave height); $k = k(x, y)$ is the wave number, and $R = R(x, y)$ the phase function, both real ($kR$ is the phase angle). Inserting (18) in (2) and putting the real part equal to zero, yields the following results for a refraction solution to be valid:

$$\left(\frac{\nabla(cc_g)}{kcc_g}\right) \cdot \left(\frac{\nabla A}{kA}\right) \ll 1 \tag{19}$$

and

$$\frac{\nabla^2 A}{k^2 A} \ll 1 \tag{20}$$

Condition (20) is well-known; (19) is probably new. The substance of (19) can be evaluated by looking at shallow water waves (for the complete result, see Reference 18). With $cc_g \approx gh$, (19) gives

$$\frac{|\nabla h|}{kh}\frac{|\nabla A|}{kA} \ll 1 \tag{21}$$

while (20) *generally* can be written

$$\kappa_A \ll \tfrac{1}{2}k^2 A \tag{22}$$

In (22) $\kappa_A$ is the local mean curvature of the amplitude surface. So it appears that a refraction approach puts restrictions on the *slope* as well as on the *curvature* of the amplitude surface ($|\nabla A|$ is the maximum local slope of the $A$-surface). It is interesting to note, however, that the slope of the amplitude surface appears *together* with the slope of the sea bed $|\nabla h|$, so that their product must be small, see (21). This is an extension of the criterion suggested in papers I and II, that $|\nabla h|$ be small compared with $kh$. If, for instance, $|\nabla A|/(kA)$ is very small, the requirements to the bed slope are less strict. The opposite is met if $|\nabla A|/(kA)$ is large.

It is seen from (21) and (22) that refraction theory cannot hold for long waves ($k$ small), large bed slopes ($|\nabla h|$ large), or along shadow boundaries ($|\nabla A|$ and $\kappa_A$ large). The last result is well-known. The first, however, is less obvious. The conclusion is that refraction theory will give increasingly poor results as the period increases. In paper II it was concluded (p. 54) that generally refraction theory is too primitive for waves in the tsunami range. In the present paper we shall elaborate on this by presenting limiting wave periods (where the number of orthogonals jumps by two) for the point Q, and by looking in some detail upon the vector addition for IDT for the points Q and P.

It should be observed that for the present we cannot say *how* small the quantities on the left-hand sides of (19) and (20) should be. Only a study of some 'canonical' cases can reveal this. It is further noted that, using (19) and (20), the imaginary part of (2), with (18) inserted, put equal to zero naturally gives the energy equation, energy flux being constant between neighbouring orthogonals (dissipation is neglected).[18]

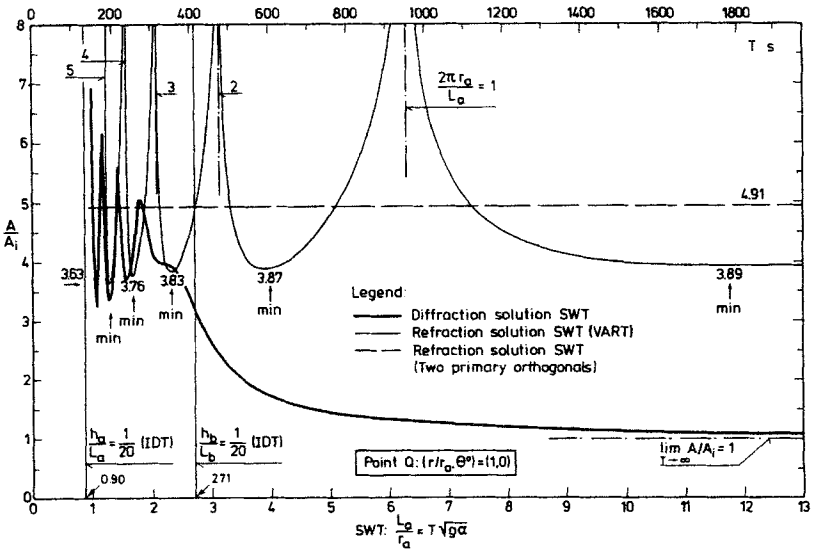


Figure 15. Relative amplitude $A/A_i$ at the point Q *vs* wave period $T$ and relative wavelength $L_a/r_a$ using shallow water theory. VART is the complete refraction solution (Vector Addition Refraction Theory)

A more complete exposition of the foundation of geometrical optics has been given by Arley[20] who further found that the wave front curvature must be small compared with $L^{-1}$ for a refraction approach to be valid.

We shall first look at the shallow water solution for the point Q. The complete (VART) SWT refraction solution for the middle island shadow point Q is shown for the first time in Figure 15. (The similar curve for the point P is shown in Figure 7 in paper I, and in Appendix IV). VART stands for Vector Addition Refraction Theory. Following the same line of argument as in paper I p. 488) it appears that here also the solution diverges for $2\pi r_a/L_a = p$ being an integer. The first four 'peak periods' are then $T = 951{\cdot}72$ s ($p = 1$), $T = 475{\cdot}86$ s ($p = 2$), $T = 317{\cdot}24$ s ($p = 3$), and $T = 237{\cdot}93$ s ($p = 4$). The complete SWT refraction solution is seen generally to have no similarity to the diffraction solution. There is some resemblance between the 'resonance' periods, though. It appears that the peaks in $A/A_i$ (Figure 15) at these 'resonance' periods are located to the right of corresponding peaks in the shallow water diffraction solution. This is commented upon in paper I (p. 489). The difference in peak period is smallest for $p$ large (small $T$). However, the agreement is weaker than for the point $P$, see paper I, Figure 7, and Appendix IV.

Using intermediate depth theory (IDT), the point Q is met by a finite number of orthogonals. Figure 16 shows the first three (six) limiting spirals for this point (they are tangent to the island at that point). Thus for $T < 58{\cdot}42$ s, no orthogonals reach the point Q. For $58{\cdot}42\text{ s} \leq T < 167{\cdot}04$ s it is reached by two (symmetrical) orthogonals, for $167{\cdot}04\text{ s} \leq T < 286{\cdot}97$ s by four orthogonals, for $286{\cdot}97\text{ s} \leq T < 409{\cdot}67$ s (not shown in the figure) by six orthogonals, and so on. For any finite period the number of orthogonals is finite (using IDT); it increases with increasing $T$ and the number tends to infinity as the period goes to infinity. It is not surprising, then, that shallow water theory gives an infinite number of orthogonals (see paper I).

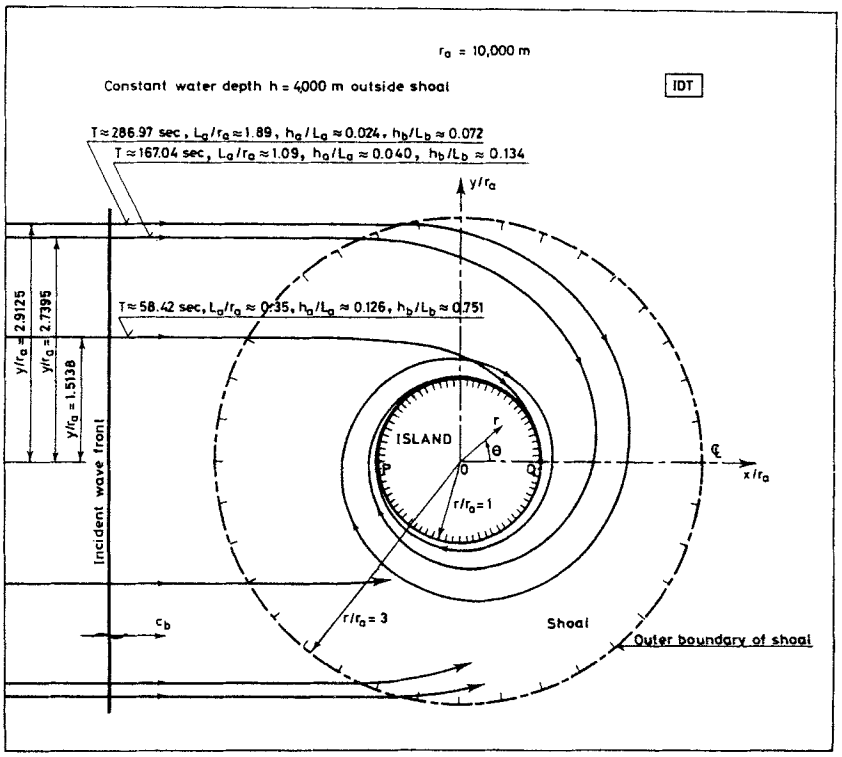


Figure 16. Limiting orthogonals for the point Q with corresponding limiting periods. Symmetrical orthogonals starting below the $x$-axis not shown in full

In Figure 9 we can follow the complete IDT refraction solution for the point Q up to about $h_a/L_a = 1/20$. Following the comments to Figure 16 the refraction solution for $T < 58{\cdot}42$ s gives zero amplitude here. Then the point is suddenly met by two orthogonals, and the relative amplitude jumps up to about 2 (also hinted at in Figure 10). By further increasing the period two interesting results are derived. Firstly, the refraction solution for the point Q does not oscillate as long as this point is met by only two orthogonals (see later for comments). Secondly, in the region viewed the refraction solution is an approximate upper bound for the diffraction solution.

In conclusion, neither refraction approach (SWT or IDT) can be said to give a reliable representation of the 'true' solution for the point Q, the diffraction solution.

Further information about the IDT refraction solution can be found by looking at the results for the point P, Figure 4 in paper II, see Appendix IV. It appears from this figure that as the number of orthogonals meeting the point jumps from one to three, the IDT refraction solution starts to oscillate. (The absence of oscillations in the short-period refraction solution is also illustrated in Figure 11.) Since the important thing at this jump is that the point is now met by orthogonals whose amplitudes are not all in phase (see Figure 18), it could be speculated that oscillations would also be found in Figure 9 had we continued the IDT refraction solution beyond $T = 167{\cdot}04$ s. Still, inspecting Figure 4 in paper II (also Appendix

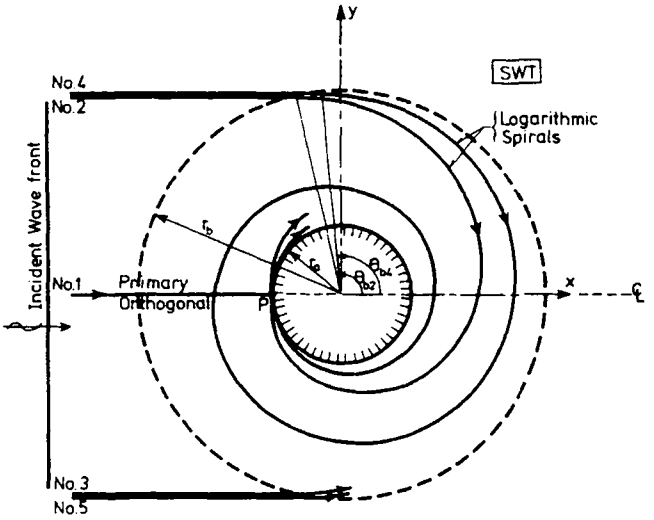


Figure 17. The first five orthogonals reaching the point P, showing two of them being reflected (SWT)

IV) once more leaves no hope for meeting a refraction solution which is a close approximation to the diffraction solution here.

Let us finally compare vector additions for SWT and IDT refraction solutions for the point P. Generally, following an orthogonal to the shoreline, the relative amplitude pertaining to this orthogonal is

$$\frac{A}{A_i} = K'_{ra} K'_s (1 + K_r) \tag{23}$$

Here $K'_{ra}$ is the modified refraction coefficient (gives the effect of orthogonal convergence or divergence), $K'_s$ is the modified shoaling coefficient (gives the effect of changing water depth), and $K_r$ is the reflection coefficient (here assumed equal to one). Examples of reflected orthogonals are shown in Figure 17. Phase angles are determined by integrating $ds/c$ along the orthogonals, $s$ being distance. Further details are given by Skovgaard *et al.*[21] and in paper I.

Some results are presented in Figure 18. Starting with (a) we look at a period very close to, but slightly below, the one where the point F is reached by three orthogonals. The vector corresponds to the primary orthogonal. At (b) we have just reached the period when the number of orthogonals becomes three. The contributions from the second and third orthogonals (marked '2' and '3') are equal, since these orthogonals are symmetrical. The result is a jump in $A/A_i$, shown in Figure 4 in paper II, and in Appendix IV. (Increasing $T$ a little more affects the phase angle for '2' and '3' stronger than that for '1'; this probably explains why $A/A_i$ can oscillate as shown in this figure.)

In (a) and (b) it would be physically absurd to include an SWT solution. This is done in (c) and (d), however. In (c) we have just passed a period (237·93 s) when the SWT solution diverges. Still, the resulting amplitude has decreased considerably, being (by chance) quite close to the IDT solution. The latter is the sum of five contributions, see Figure 19. The

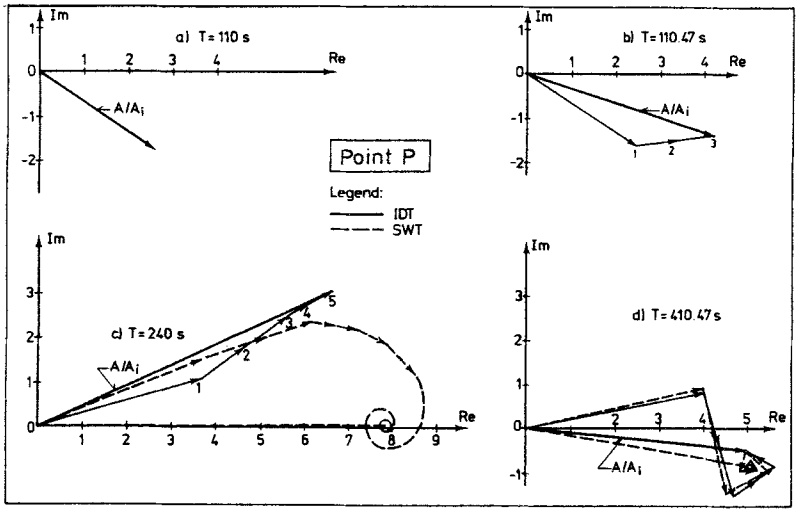


Figure 18. Vector addition of wave surface displacements at the point P from a refraction calculation. IDT and SWT

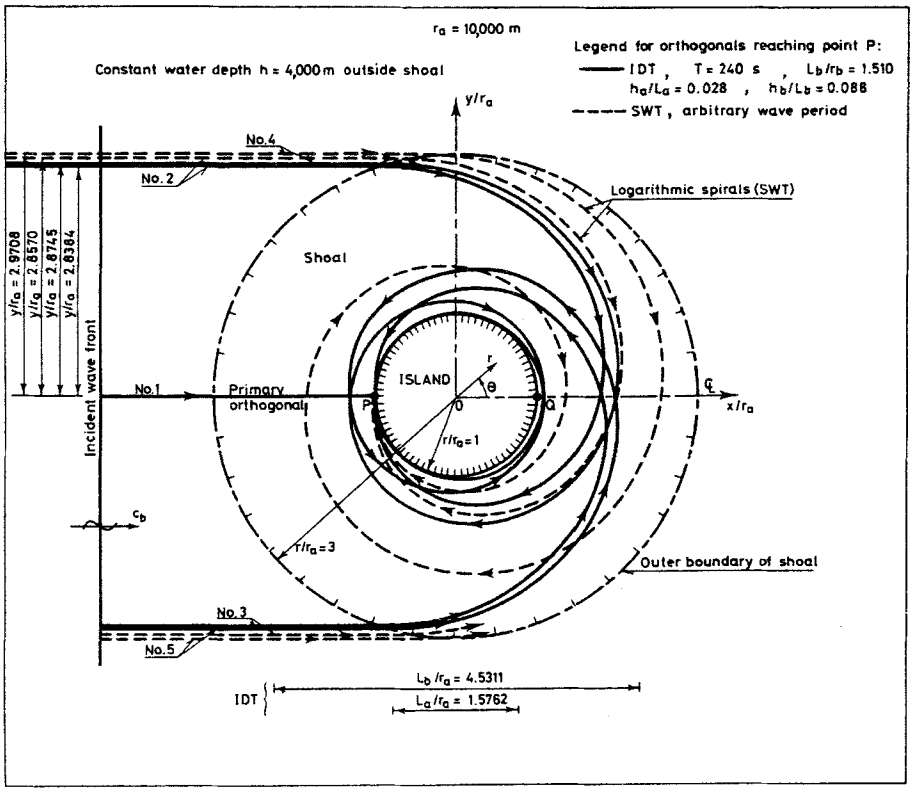


Figure 19. Orthogonals reaching the point P for $T = 240$ s (Only the first five SWT orthogonals shown)

higher the orthogonal number, the smaller the refraction coefficient and thus the amplitude contribution. Finally (d) illustrates conditions in the shallow water limit $T = 410{\cdot}47$ s, corresponding to $h_b/L_b = 1/20$. The difference between the IDT and SWT solutions is quite small, in amplitude as well as in phase angle.

The small deviations between the IDT and the SWT solutions in (c) and (d) in Figure 18 should not lure one into believing that this is a general trend. This is evident from the fact alone that the SWT solution can diverge; the IDT ditto cannot. See also the four IDT amplitude points in paper II, Figure 4 (also in Appendix IV), and the two VART–SWT surface displacements at point P around $L_a/r_a = \frac{2}{3}\pi r_a$ in paper I, Figure 11 (also in Appendix IV).

The orthogonal paths resulting in (c) in Figure 18 are depicted in Figure 19.

The IDT refraction solution along the island circumference is shown in Figure 8 for $T = 120$ s. The primary orthogonal gives a kind of moving average of the diffraction solution, with no oscillations present. The complete refraction solutions for the point P (three orthogonals) and the point Q (two orthogonals) are also shown. The latter gives the same amplitude as the diffraction solution. This is a coincidence, however, as can be seen from Figure 9.

## 5. ISLAND WITHOUT A SHOAL

In this section we shall illustrate the influence of the shoal by looking at a few cases of a circular cylindrical island in an ocean of constant depth, i.e. without a shoal. In Figures 20 and 21 wavelength $L$ is related to island radius $r_a$; the 'corresponding' wave periods depend on the choice of water depth and island radius. To be able to make a direct comparison with previous figures we choose $h = h_b = 4{,}000$ m here and $r_a = 10$ km.

Since water depth is now constant, there is neither 'shoaling' nor 'refraction'; what we have is simply 'diffraction in a homogeneous medium'. This means that there is less 'trapping' of wave energy at the island, which is especially noticeable when one looks at conditions in the shadow part of the island. In front of the island we have only partial reflection; this is due to the curvature of the shoreline. The result is a modified standing wave. Also the amphidromic points vanish in the absence of an increasing water depth away from the island.

The diffraction patterns in Figures 20 and 21 are solutions to the Helmholtz equation (10), since phase speed is constant here.

In Figure 20 we have depicted amplitudes and phase angles for a large water area, corresponding to the longest period under investigation, $T = 480$ s. Comparison with Figure 3 (same period, *with* shoal) shows generally a much less disturbed wave field. As an example the deep minimum in the upper right-hand part of Figure 3 is missing in Figure 20.

For this rather long wave (as compared with island size) the relative amplitudes in the middle of the shadow region (i.e. along the positive $x$-axis) come very close to the limiting value—unity—for $T$ tending to infinity. In the presence of the shoal (Figure 3), however, the waves are 'bent' around the island, and much higher amplitudes are found here. The limiting value, $A/A_i = 1$ for $T \to \infty$, is common for the two cases, see for instance paper II, Figure 5, and Appendix IV. In the limit $T \to 0$, the amplitude vanishes at the point Q (and further along the positive $x$-axis), see Figure 10 and paper II, Figure 5 (Appendix IV).

In the middle of the 'illuminated' region (i.e. along the negative $x$-axis), deviations from unity of relative amplitude are smaller in Figure 20 than in Figure 3, as expected; there is more reflection in the latter case, naturally. The large difference in amplitude at the point P

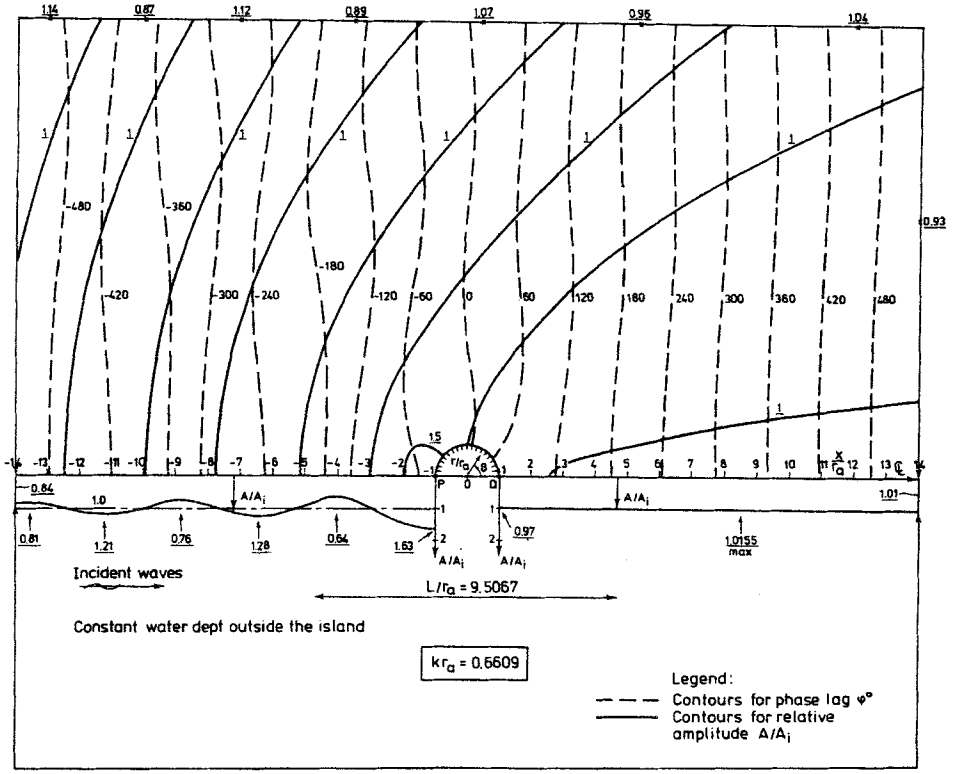


Figure 20. Contours for relative amplitude $A/A_i$ and phase angle $\varphi$ for a cylindrical island in an ocean of constant depth. For $h = 4{,}000$ m, and $r_a = 10$ km, $T = 480$ s. The interval between the $A/A_i$-curves is 0·5, and between the $\varphi$-curves is 60°. Underlined numbers are $A/A_i$

is due to 'shoaling' and 'refraction' effects in the case of a shoal (Figure 3). For $T$ going to infinity, the relative amplitude approaches unity here, with or without a shoal, see paper I, Figure 7, and Appendix IV. In the limit $T \to 0$, we have full reflection at the point P (and, further, neither shoaling nor refraction in the case of a shoal), and so in both cases $A/A_i = 2$, see Figure 11 and paper II, Figures 4 and 11, Appendix IV in this paper.

In Figure 21 we have almost deep water waves for $h = 4{,}000$ m and $r_a = 10$ km, since this gives $h/L \approx 0{\cdot}51$. The corresponding period is $T \approx 71$ s. For this small wavelength (as compared with island radius) we have nearly full reflection in front of the island, and quite small amplitudes in the lee of it. The deviation between Figures 20 and 21 is marked in this respect. (Note when comparing that in Figure 21 we have omitted to show the curves for $A/A_i = 1{\cdot}5$—shown in Figure 20—and $A/A_i = 0{\cdot}5$. So in reality there is a 'hole' behind the island in Figure 21. 'deeper' than $A/A_i = 0{\cdot}5$.)

In paper II, Figure 10 we have shown amplitudes and phase angles for a wavelength between those in the present Figures 20 and 21; the period in the above-mentioned figure is $T = 174$ s for $h = 4{,}000$ m, and $r_a = 10$ km.

The variation for continuous periods is shown in paper II, Figure 11 (and in Appendix IV) for point P. (Note, though, that in the figure periods $T$ corresponds to $h = h_a = 444$ m. The

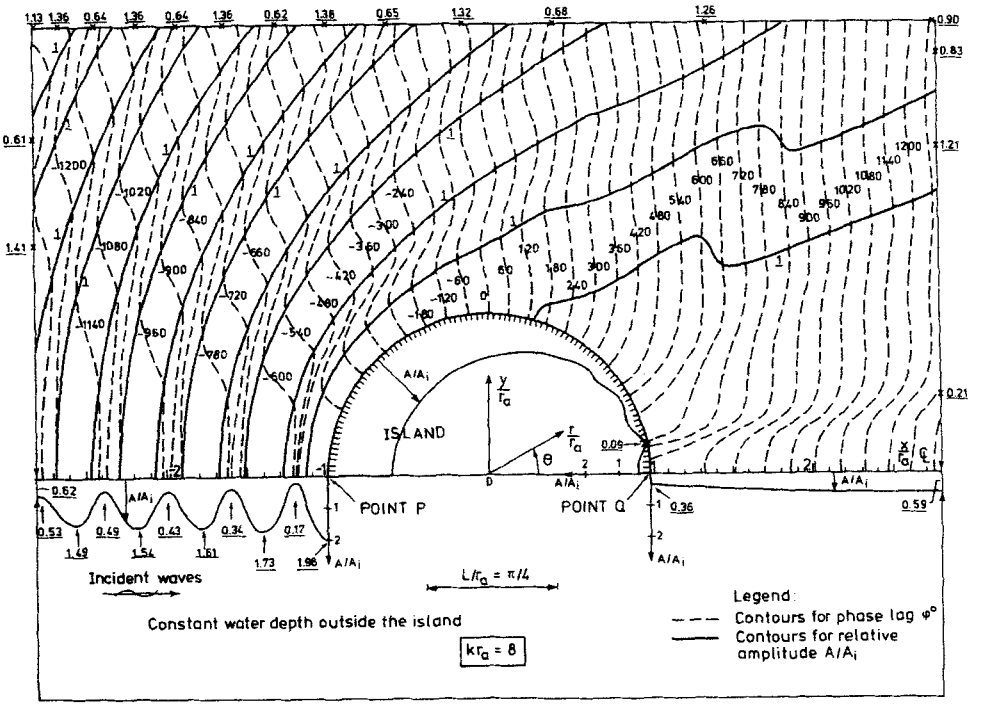


Figure 21. Contours for relative amplitude $A/A_i$ and phase angle $\varphi$ for a cylindrical island in an ocean of constant depth. For $h = 4{,}000$ m, and $r_a = 10$ km, $T \approx 71$ s. The interval between the $A/A_i$-curves is 1, and between the $\varphi$-curves is 60°. Underlined numbers are $A/A_i$

transformation of the $T$-axis to $h = h_b = 4{,}000$ m is trivial, however.) An expanded view for small periods is shown in the present Figure 11.

The variation for continuous periods for the point Q is shown in Figure 10. Also here note that in the figure periods $T$ correspond to $h = h_a = 444$ m.

## 6. CONCLUSION

A number of complete linear refraction and diffraction solutions have been presented for the sea surface in the neighbourhood of the island shown in Figure 1. The incident (tsunami) waves are assumed plane, regular, and of small amplitude, and the sides of the island fully reflecting. Dissipation is neglected, as is the Coriolis force.

The paper is a sequel to two previous contributions by the authors, Jonsson *et al.*[10] (paper I), and Jonsson and Skovgaard[11] (paper II). Paper I was restricted to the presentation of the wave field at the shoreline of the island, while paper II concentrated on the wave field over the shoal, for periods in the upper end of the tsunami frequency range (wave periods 120 and 240 s). Refraction calculations (only for the shoreline) were extensively discussed and presented for Shallow Water Theory (SWT ~ 'long waves') in paper I, while in paper II some steps were taken towards an Intermediate Depth Theory (IDT ~ 'short waves') refraction solution.

The present study is therefore primarily directed towards the following three subject areas: (i) The wave field in the ocean of constant depth far away from the island and shoal; (ii) the wave field over the shoal for a larger wave period ($T = 480$ s); (iii) refraction calculation results for two selected points at the shoreline (P and Q in Figure 1) using an IDT Vector Addition Refraction Theory (VART). The result is a large number of very accurate numerical results, to a great extent presented in graphical form, and two test solutions are tabulated.

For items (i) and (ii) solutions are found using a so-called mild-slope wave equation (based on IDT), which is correct to first order in both wave steepness and bed slope. The resulting amplitude-phase figures show among other things that the number of amphidromic points (where the amplitude vanishes) decreases with increasing period; for $T = 480$ s they are totally absent. It is further found that amphidromic points can exist, not only over the shoal but also outside it, in the water area of constant depth. The amplitude out at sea can be quite large compared with that of the incoming wave.

The influence of the shoal is studied by looking at the diffracted wave field around a circular cylindrical island in an ocean of constant depth (solutions to the Helmholtz equation); generally the wave field is less 'disturbed' in the absence of the shoal. This is illustrated by the fact that we do not find amphidromic points here (since the Coriolis force is neglected). With the shoal present the amplitudes near the island can be several times the incident wave.

The continuous variation with wave period of the amplitudes in the points P and Q (see Figure 1) is studied and illustrated in great detail for the smaller period values. The diffraction solution is found here to be well represented by the result of a refraction approach for small wave periods ($T < 35$ s for the point P, somewhat less for the point Q). The rapidly growing oscillations of the amplitude *vs* period for longer periods is illustrated for the point P in a quite staggering figure (Figure 11).

For the point Q the variation of amplitude with period is further followed up to $T = 500$ s (Figure 9).

The conclusion is the same as in paper II, that the SWT diffraction solution (i.e. using the linearized shallow water wave equation) is a very good approximation to the 'true' solution (IDT) for $T$ larger than 7 min (with the reservation, naturally, that linear theory holds; see the comments in the introduction). The SWT amplitudes diverge more and more from the IDT solution as the period decreases. However, if a high degree of accuracy is not needed, one can use the much simpler SWT approach down to, say, $T = 5$ min.

The convergence rate of the series used for the solution of the wave equations is investigated in Appendix I. For a fixed accuracy, the necessary number of terms $n_{max}$ in the series is shown to increase with increasing distance from the island and (rapidly) with decreasing period. The programming for the numerical calculations is briefly outlined in Appendix II.

A new criterion—based on the IDT wave equation—for the applicability of a refraction approach is summarized. The result is that the product of a relative bed slope and a relative slope of the amplitude surface be small (as well as the curvature of the amplitude surface, which is well known).

In paper I the complete (i.e. VART) SWT refraction solution was presented for the point P (amplitude *vs* period). It was shown that the vector addition in this case involved an infinite number of complex amplitudes from the individual orthogonals; the series diverges for $2\pi r_a/L_a$ being an integer ($L_a$ being wavelength for $r = r_a$, the island shoreline). For completeness a similar figure is presented here for the point Q (Figure 15). Also here the refraction solution generally has very little likeness to the true (diffraction) solution.

A complete IDT refraction approach was hereafter tested; in contrast to the SWT approach it contains only a limited number of vectors, each corresponding to an orthogonal reaching the point. For the point Q we have followed it continuously up to $T \approx 120$ s (Figure 9). The figure demonstrates—together with paper II, Figure 4, see Appendix IV, dealing with discrete periods for the point P—that the 'refinement' of a complete IDT refraction solution does not repair the inadequacy of SWT refraction. The only advantage is that in the former case the resulting amplitude is bounded for any period. The conclusion is that in cases similar to the present one, the geometrical optics approach—however tempting to use presenting an initial value problem—is all too primitive for waves in the tsunami range. This means cases where the water depth varies significantly over a wavelength. It is felt that one can generally conclude that refraction calculations should be applied only with utmost reservation to such long waves as tsunamis.

All non-linear effects, including dissipation, have been neglected.

ACKNOWLEDGEMENTS

Dr. Niels Arley is acknowledged for helpful comments to the manuscript.

Liselotte Norup and Erling Poder are acknowledged for great care in the preparation of the drawings, and Kirsten Studnitz for expert typing.

## APPENDIX I: CONVERGENCE OF FOURIER SERIES FOR THE DIFFRACTION SOLUTIONS

For the practical application of the finite Fourier series for the diffraction solution (12) or (13) to (15) it is useful to know how many terms one needs in order to obtain a given accuracy. This information can be even more important when we discuss whether a certain solution approach at all can be applied in a certain period range or in a certain space region of $r$ and $\theta$.

In paper I (3.24) we introduced the number of terms $n_{max}$, necessary to obtain a prescribed relative accuracy 'eps' ($0 < \text{eps} \ll 1$), which we here define by the relation

$$\left| \sum_{n=0}^{n_{max}} R_n(r) \cos(n\theta) - \text{exact solution} \right| < \text{eps} \times A_i \tag{24}$$

or

$$|(A/A_i)_{\text{approximate}} - (A/A_i)_{\text{exact}}| < \text{eps} \tag{25}$$

This simple accuracy criterion, which directly controls the amplitudes and neglects the phases, is selected because of its simplicity. The exact solutions to (12) or (13) to (15) were constructed by continuing the summation until the last term of $|R_n/A_i|$ was less than eps squared.

Inspection of the calculated phases revealed that the approximation errors for the phases basically followed the same dependence on wave period $T$ and on the horizontal co-ordinates $r$ and $\theta$ as depicted for $A/A_i$ in the figures in this appendix.

In Figure 22 for $T = 480$ s (using the shallow water wave equation (8)) and $\theta = 0°$ (i.e. along the positive part of the $x$-axis) $n_{max}$ *vs* $x/r_a$ is shown for $1 \le x/r_a \le 28$ and for $\text{eps} = 10^{-2}$, $10^{-4}$ and $10^{-8}$. ($\text{eps} = 10^{-d}$ is normally referred to as two times $d$-places decimal accuracy.)

Similar figures have been constructed for other values of $\theta$, and from these figures we can

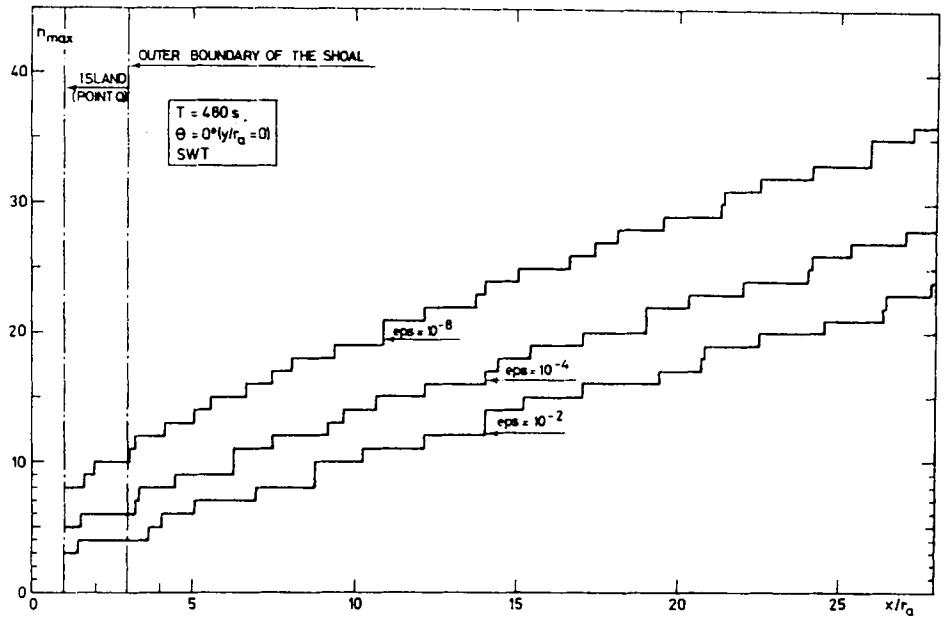


Figure 22. The necessary number of terms $n_{max}$ in the Fourier series (SWT solution) *vs* $x/r_a$ for $T = 480$ s, $1 \leq x/r_a \leq 28$ (¢ of shadow region), and eps = $10^{-2}$, $10^{-4}$ and $10^{-8}$

conclude that Figure 22 is in practice valid for arbitrary $\theta$. For a fixed $r/r_a$ the difference between $n_{max}$ in Figure 22 and the $n_{max}$ in figures for other $\theta$ was never larger than 2.

The general conclusion is that $n_{max}$ increases monotonically with $x/r_a$. For eps constant the variation is nearly linear from the island and outwards. From Figure 22 we can further conclude that for points on the shoal, $n_{max}$ is only increased by one or two (depending on eps) when we 'move' from the island to the outer boundary of the shoal. If eps is decreased from $10^{-2}$ to $10^{-4}$ only up to five additional terms are needed in the solution series for $x/r_a$ less than 28 and for $T = 480$ s (Figure 22). If eps is again squared (i.e. eps = $10^{-8}$) only up to seven additional terms are needed. (Notice that for $\theta = 0°$ all the cos $(n\theta)$ factors in (24) are equal to one.)

Similar figures to Figure 22 have been constructed for other values of wave period $T$ and from these figures we have found that if we use $x/L$ (instead of $x/r_a$) as abscissa, Figure 22 becomes in practice valid for an arbitrary SWT wave period (or wavelength $L$).

In Figure 23, for eps = $10^{-4}$ and $\theta = 0°$ (i.e. points along the positive part of the $x$-axis), $n_{max}$ *vs* $T$ is shown for 200 s $\leq T \leq$ 1900 s, and for $x/r_a = 1$, 3, 9 and 27. The figure is based on the shallow water wave equation (8).

Figures similar to Figure 23 have been constructed for other values of $\theta$, and from these figures we can conclude that Figure 23 is in practice valid for an arbitrary $\theta$.

The general conclusion is that $n_{max}$ increases with decreasing period (shorter waves). Far away from the island the increase is rapid. We can further summarize that for all periods in the SWT range, and for all points up to a distance of, say $r/r_a \approx 10$, only up to 20 terms of the series solution are needed for eps $\geq 10^{-4}$. As far as, say $r/r_a \leq 30$ only up to 40 terms are needed for eps $\geq 10^{-4}$. For solutions in any point on the shoal only up to eight terms are needed in the SWT period range for eps $\geq 10^{-4}$.

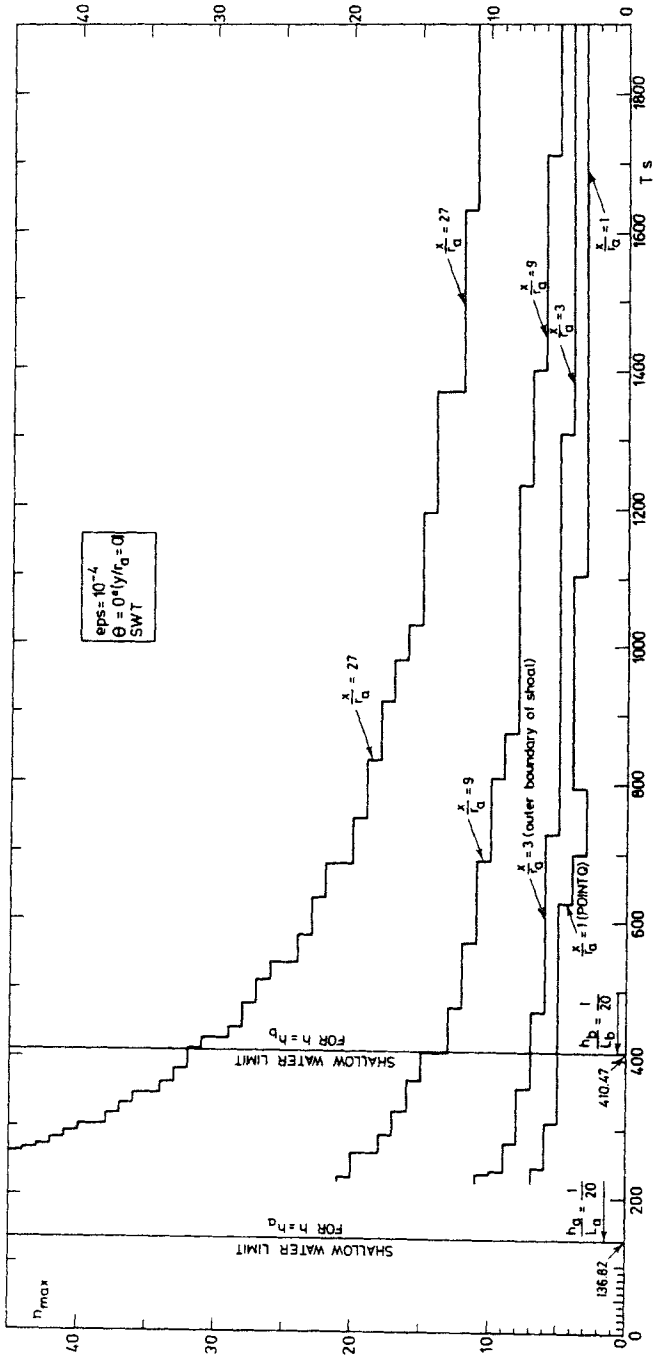


Figure 23. The necessary number of terms $n_{max}$ in the Fourier series (SWT solution) *vs* wave period $T$ for eps $= 10^{-4}$, $200 < T < 1900$ s, and $x/r_a = 1, 3, 9$ and 27 (¢ of shadow region)

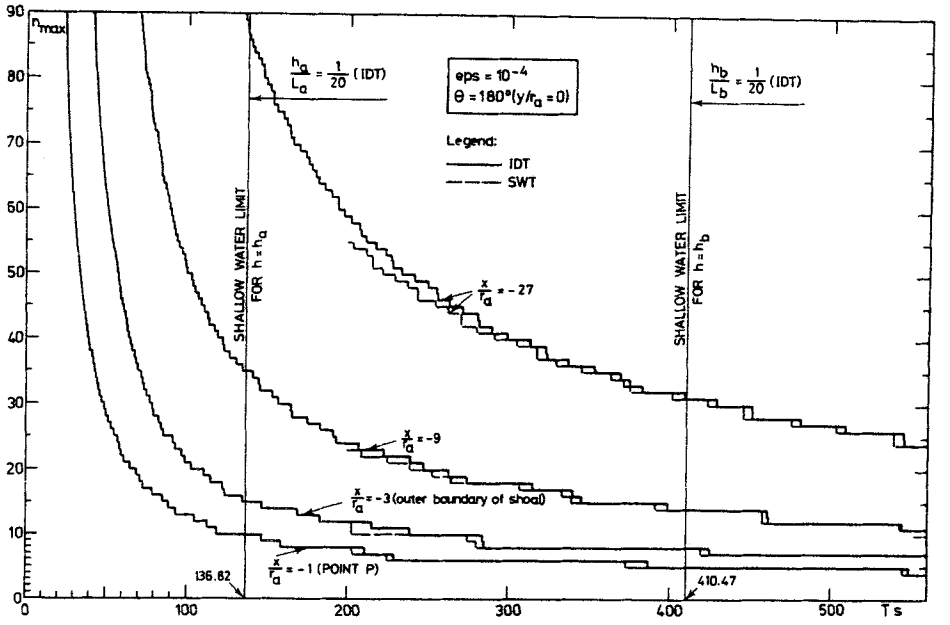


Figure 24. The necessary number of terms $n_{max}$ in the Fourier series (IDT and SWT solution) *vs* wave period $T$ for eps = $10^{-4}$, $0 < T \leq 560$ s, and $x/r_a = -1$, $-3$, $-9$ and $-27$ (℄ of 'illuminated' region)

To investigate the difference between number of terms necessary in the SWT and IDT cases, Figure 24 was drawn up. In this figure we have shown $n_{max}$ *vs* $T$ for eps = $10^{-4}$, and $\theta = 180°$ i.e. points along the negative $x$-axis), for $0 < T \leq 560$ s, and $x/r_a = -1$, $-3$, $-9$ and $-27$. The full curves correspond to solution of the intermediate depth wave equation (2).

In the shallow water period range of this figure also the results of an SWT calculation (solution to (8)) are plotted (for comparison). For $T$ larger than say, 420 s, the two sets of curves (IDT and SWT) were for continuity reasons expected to be almost identical beforehand. The figure shows that this is indeed nearly the case. For all relevant values of $T$ (i.e. say $T \geq 200$ s), the IDT and SWT curves coincide for $x/r_a = -1$ and $-3$. For $|x/r_a|$ increasing on the constant water depth, however, the SWT solution needs a few terms less than the IDT solution in the overlap range for $T$ (IDT⇔SWT, say 200 s $< T <$ 420 s).

Figure 24 also shows that for $T$ decreasing in the 'short' period range (say $T \leq 140$ s) the number of terms necessary in the Fourier series increases very quickly. For $x/r_a = -1$, $\theta = 180°$ (the point P, Figure 1), and $T \leq 20$ s, the method is impractical, demanding an unreasonable CPU (Central Processing Unit) time in the computer.

For the point P we showed in Figure 11 that for $T \leq 35$ s, the solutions of the wave equation (2) and the refraction were identical. For $T = 35$ s we see from Figure 24 that about 50 terms of the Fourier series solution of the wave equation have to be included for the point P. (In contrast to this the refraction solution for this period (and all smaller periods) had a contribution from only one orthogonal, i.e. consisted of only one term, so to speak.)

Here we must stress that it is only for points along the 'illuminated' part of the shoreline of the island that, in the period range where the Fourier series solution becomes impractical, we have presented another method (the refraction approach) to determine the wave field. An

alternative method for small periods and for all other points than the above-mentioned 'illuminated' part of the shoreline is therefore needed.

More refined ray methods, such as Keller's geometrical diffraction theory (GDT, see References 22 and 23) have been developed only for constant water depth, or for variable water depth using SWT, and in the latter period range we have already an efficient analytical solution to (8), see (3.6) together with (3.19) in paper I. In principle it may be possible to extend the GDT method to variable water depth using IDT, but the ray tracing is likely to become so cumbersome that the method becomes impracticable.

A more promising method for small periods is to look for an alternative method to sum the slowly converging series (12) or (13) to (15). From Figure 24 we concluded that it was impracticable to compute the sum of the series by adding up the terms. The usual method of summing a slowly converging series $\sum_{n=0} a_n$ is to *replace* it with a series $\sum_{n=0} b_n$ which has the property that its partial sums $s_m = \sum_{n=0}^{m} b_n$, for small values of $m$, give good approximations to the sum of the series $\sum_{n=0} a_n$. The series $\sum_{n=0} b_n$ may be either convergent or divergent. These methods are very attractive[24] and may be investigated in a later publication.

## APPENDIX II: PROGRAMMING

The numerical methods described were programmed in the IBM OS 370 implementation of PL/I using version 1 of the PL/I optimizing computer.[25] The programs were executed at the computing centre (NEUCC) at the Technical University of Denmark, using an IBM 370/165, and from July 1979 on an IBM 3033.[26–28]

The floating-point calculations of the vector addition refraction theory (VART) in Section 4.2 were programmed in extended precision, which for the above-mentioned computer is 28 hexadecimal digits (approximately 35 decimal digits). All other floating-point calculations were made in double precision, i.e. 14 hexadecimal digits (approximately 16 decimal digits).

## APPENDIX III: ABBREVIATIONS

Paper I = Jonsson *et al.*[10]
Paper II = Jonsson and Skovgaard.[11]
Point P = the middle of the front face of the island (Figure 1).
Point Q = the middle of the shadow region of the island (Figure 1).
SWT = shallow water theory.
IDT = intermediate depth theory.
VART = vector addition refraction theory.
Suffix *a* refers to quantity at the island shoreline (inner edge of the shoal).
Suffix *b* refers to quantity at the outer edge of the shoal.
Suffix 'i' refers to undisturbed (incident) wave on constant water depth.
$L_0$ = deep water wavelength, see (11).

# APPENDIX IV: REPRINTS OF 8 FIGURES FROM PAPERS I AND II

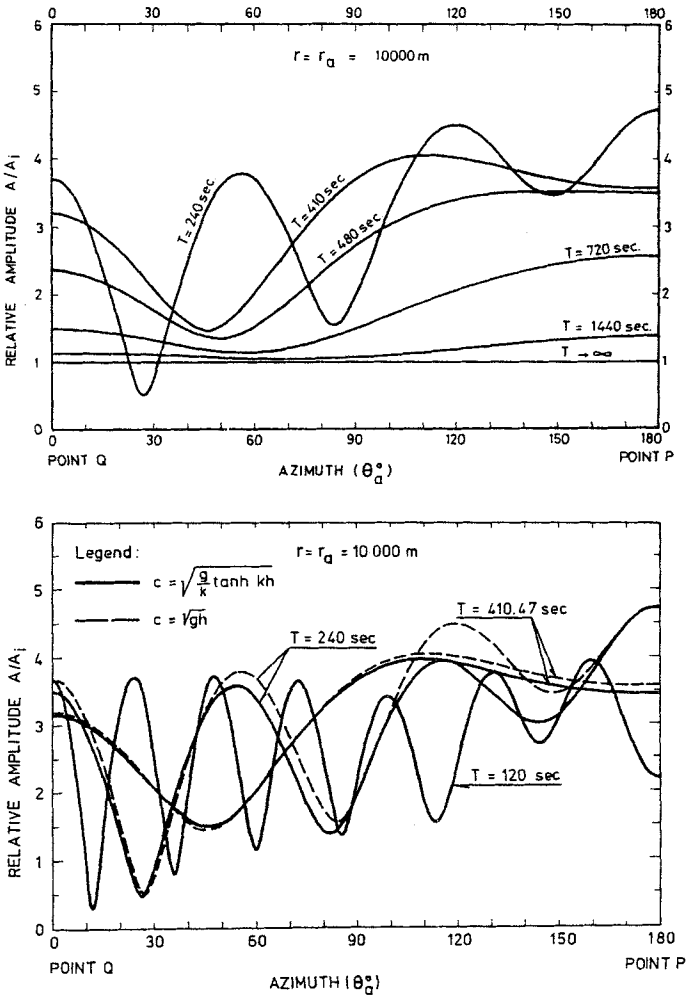


Figure 2 in paper I. Relative amplitude $A/A_i$ at shoreline *vs* azimuth $\theta_a^\circ$: (a) (top) Corresponding to an analytical shallow water diffraction solution; (b) (bottom) Corresponding to a numerical intermediate depth diffraction solution and two curves from (a)

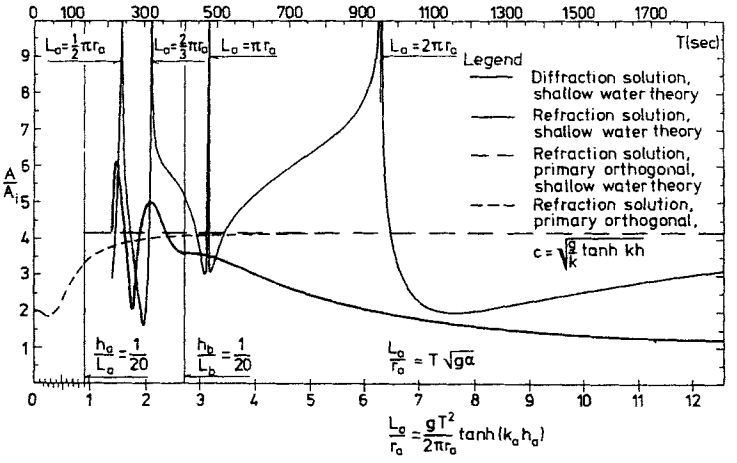


Figure 7 in paper I. Relative amplitude $A/A_i$ at point P *vs* wave period $T$ and relative wavelength $L_a/r_a$. Analytical shallow water diffraction and refraction solutions, and numerical intermediate depth refraction solution for the primary orthogonal

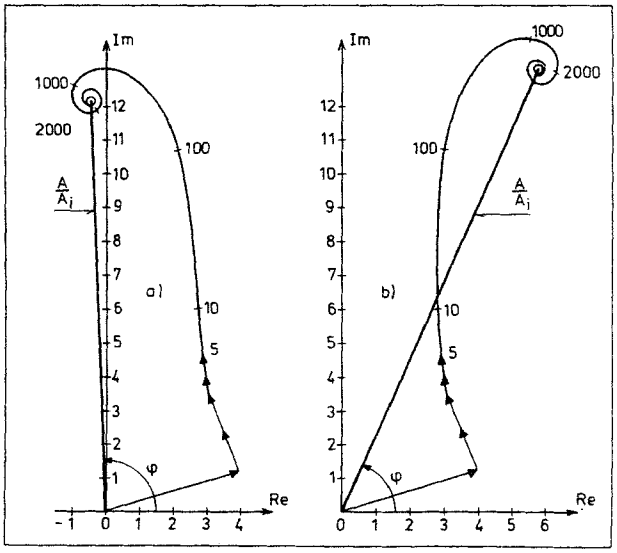


Figure 11 in paper I. Vector addition of wave surface displacements at point P due to a shallow water refraction solution; (a) $T = 317{\cdot}15$ s; (b) $T = 317{\cdot}30$ s

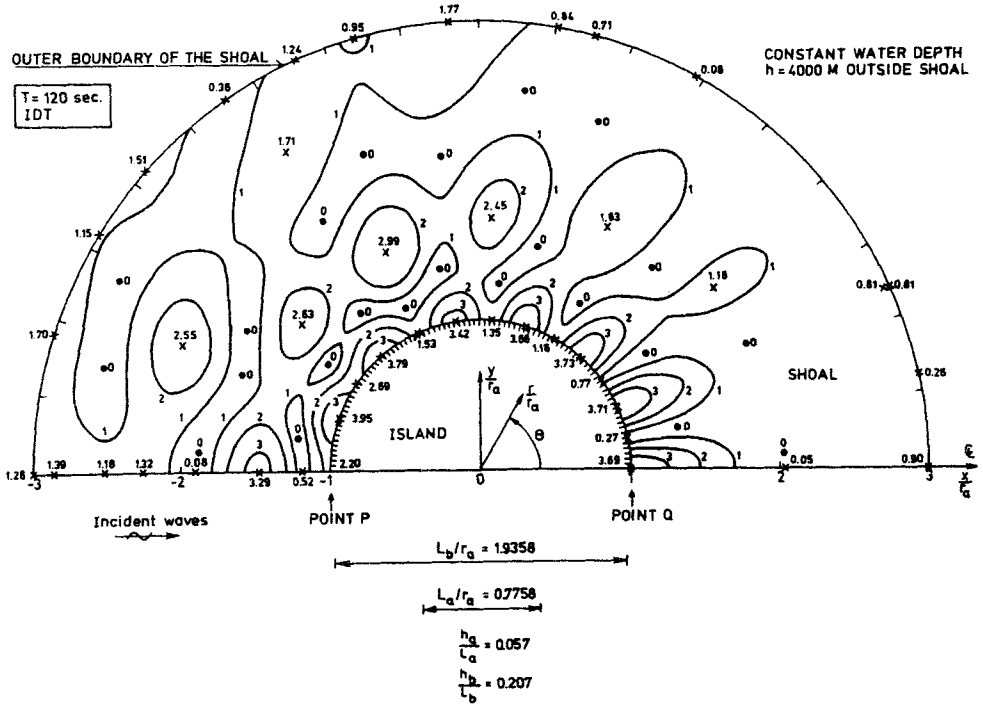


Figure 3 in paper II. Contours for relative amplitude $A/A_i$ over the shoal. $T = 120$ s. The interval between the $A/A_i$ curves is 1

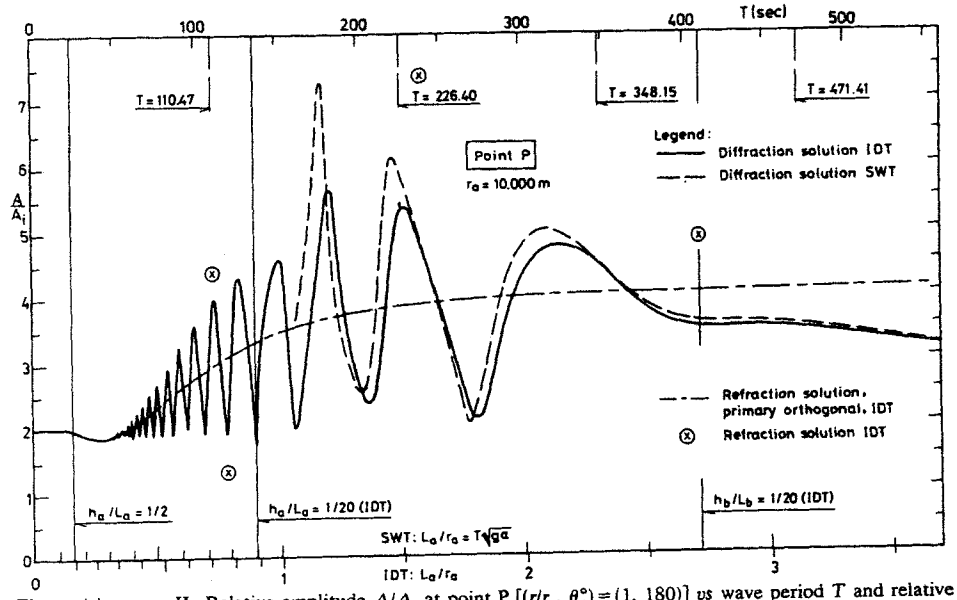


Figure 4 in paper II. Relative amplitude $A/A_i$ at point P $[(r/r_a, \theta_a^\circ) = (1, 180)]$ *vs* wave period $T$ and relative wavelength $L_a/r_a$

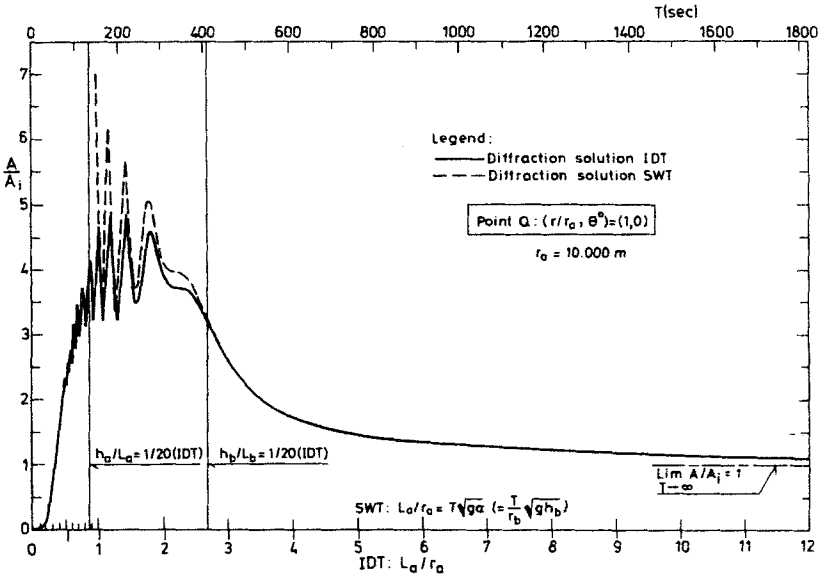


Figure 5 in paper II. Relative amplitude $A/A_i$ at point Q $[(r/r_a, \theta_a^\circ) = (1, 0)]$ *vs* wave period $T$ and relative wavelength $L_a/r_a$

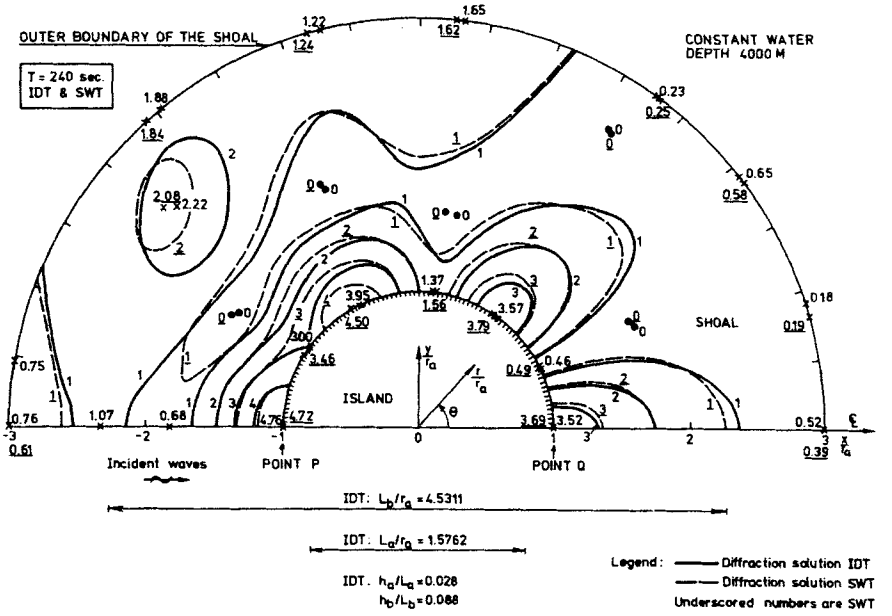


Figure 6 in paper II. Contours for relative amplitude $A/A_i$ over the shoal corresponding to both IDT and SWT. $T = 240$ s

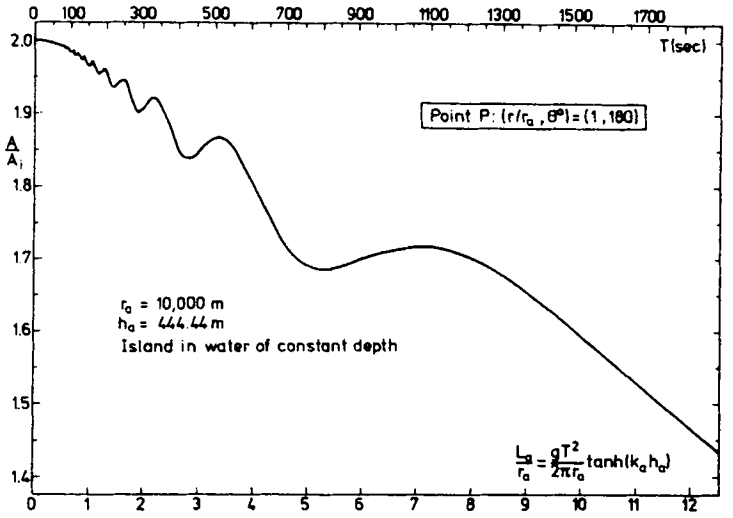


Figure 11 in paper II. Relative amplitude $A/A_i$ at point P $[(r/r_a, \theta_a^\circ) = (1, 180)]$ *vs* relative wavelength $L_a/r_a$ for a cylindrical island in an ocean of constant depth. Periods $T$ correspond to $r_a = 10{,}000$ m and $h = h_a \approx 444$ m

Figures from paper I reprinted from *J. Mar. Res.*, **34** (3), 469–496, by permission of the Sears Foundation for Marine Research, Yale University, New Haven, Connecticut, 1976.

Figures from paper II reprinted from *Mar. Geodesy*, **2**(1), 41–58, by permission of Crane, Russak & Co., Inc. © 1979 by Crane, Russak & Co., Inc., New York.

## REFERENCES

1. T. S. Murty, 'Seismic sea waves. Tsunamis', *Bull. 198*, Dept. of Fisheries and the Environment, Fisheries and Marine Service, Scientific Information and Publications Branch, Ottawa, x + 337 pp. + Appendix (41 pp., microfiche) (1977).
2. F. E. Camfield, 'Tsunami engineering', *Special Report No. 6*, U.S. Army Coastal Engrg. Res. Center, U.S. Government Printing Office, Washington, D. C. (1980). 222 pp.
3. S. Homma, 'On the behaviour of seismic sea waves around circular island', *Geophys. Mag.*, **21**, 199–208 (1950).
4. A. C. Vastano and R. O. Reid, 'Tsunami response for islands: verification of a numerical procedure', *J. Mar. Res.*, **25**, 129–139 (1967).
5. R. E. Meyer, 'Resonance of unbounded water bodies', in *Mathematical Problems in the Geophysical Sciences* (Ed. W. H. Reid), Am. Math. Soc. Lect. in Appl. Math., Vol. 13, 189–227, 1971.
6. R. Smith and T. Sprinks, 'Scattering of surface waves by a conical island', *J. Fluid Mech.*, **72**, 373–384 (1975).
7. G. A. Kriegsmann, 'An illustrative model describing the refraction of long water waves by a circular island', *J. Phys. Ocean*, **9**, 607–611 (1979).
8. J. A. Williams and T. D. K. Kartha, 'Model study of long-wave amplification by circular islands', *Bull. Seism. Soc. Amer.*, **59**, 299–316 (1969).
9. D. G. Provis, 'Experimental studies of wave refraction', in *Waves on Water of Variable Depth* (Ed. D. G. Provis and R. Radok), Lecture Notes in Physics, Vol. 64, 39–45, 1977, Springer-Verlag, Berlin.
10. I. G. Jonsson, O. Skovgaard and O. Brink-Kjaer, 'Diffraction and refraction calculations for waves incident on an island', *J. Mar. Res.*, **34**, 469–496 (1976). (*Paper I.*)
11. I. G. Jonsson and O. Skovgaard, 'A mild-slope wave equation and its application to tsunami calculations', *Mar. Geodesy*, **2**, 41–58 (1979). (*Paper II.*)
12. I. A. Svendsen, 'The wave equation for gravity waves in water of gradually varying depth', Coastal Engrg. Lab. and Hydraulic Lab., Tech. Univ. Denmark, *Prog. Rep. No. 15*, 2–7 (1967).
13. J. C. W. Berkhoff, 'Computation of combined refraction–diffraction', in *Proc. 13th Coastal Engng Conf.*, Vancouver (1972). *ASCE*, New York, Vol. 1, chapter 24, 471–490.

14. J. C. W. Berkhoff, 'Linear wave propagation problems and the finite element method', in *Finite Elements in Fluids* (Ed. R. H. Gallagher, J. T. Oden, C. Taylor and O. C. Zienkiewicz), Vol. 1, Wiley, Chichester, 1975, pp. 251–264.
15. J. C. W. Berkhoff, 'Mathematical models for simple harmonic linear water waves: wave diffraction and refraction', Delft Hydraulic Laboratory, *Publ. No. 163* (1976), 112 pp.
16. I. G. Jonsson and O. Brink-Kjaer, 'A comparison between two reduced wave equations for gradually varying depth', Inst. Hydrodyn. and Hydr. Engng (ISVA), Tech. Univ. Denmark, *Prog. Rep. No. 31*, 13–18 (1973).
17. O. Skovgaard and I. G. Jonsson, 'Transient finite-difference tsunami calculations', *Proc. 17th Coastal Engng Conf.*, Sydney (1980) *ASCE*, New York (1981).
18. I. G. Jonsson, 'The general wave equation and the refraction approximation', Inst. Hydrodyn. and Hydr. Engng (ISVA), Tech. Univ. Denmark, *Prog. Rep. No. 49*, 11–20 (1979).
19. M. Kline and I. W. Kay, *Electromagnetic Theory and Geometrical Optics*, Interscience, New York, 1965, xii+527 pp.
20. N. Arley, 'A note on the foundations of geometrical optics', *Kgl Danske Videnskab Selskab, Mat-Fys*, **22**, 1–21 (1945).
21. O. Skovgaard, I. G. Jonsson and J. A. Bertelsen, 'Computation of wave heights due to refraction and friction', *Proc. ASCE, J. Waterways, Harbors and Coastal Engng Div.*, **101**, WW1, 15–32 (1975). (*Closure*, **102**, WW1, 100–105 (1976)).
22. P. L. Christiansen, 'Diffraction of gravity waves by large islands', *Proc. 14th coastal Engng Conf.*, Copenhagen (1974), Vol. 1, Chapter 34, 601–614, *ASCE*, New York, 1975.
23. P. L. Christiansen, 'Diffraction of gravity waves by ray methods', in *Waves on Water of Variable Depth* (Ed. D. G. Provis and R. Radok), Lecture Notes in Physics, Vol. 64, 28–38, 1977, Springer-Verlag, Berlin.
24. R. Johnsonbaugh, 'Summing an alternating series', *Am. Math. Monthly*, **86**, 637–648 (1979).
25. IBM, *OS PL/I Checkout and Optimizing Compilers: Language Reference Manual*, File No. S360/S370–29. Order No. GC33–0009–4, IBM, White Plains, New York, 1976, xiv+545 pp.
26. *IBM System/370; Principles of Operation*, File No. S/370–01. Order No. GA22–7000–5, IBM, White Plains, New York, 1976, viii+326 pp.
27. IBM, *A Guide to the IBM System/370 Model 165*, File No. S370–01. Order No. GC20–1730–4, IBM, White Plains, New York, 1976, vi+162 pp.
28. IBM, *IBM 3033 Functional Characteristics*, File No. S370–01. Order No. GA22–7060–3, IBM, White Plains, New York, 1979, vi+33 pp.